Design of Fiber Networks for Studying Metastatic Invasion

14

Apratim Mukherjee, Aniket Jana, Brian Koons, and Amrinder Nain

Abstract

Cancer metastasis, the dissemination of cancer cells from the primary tumor site to distal organs in the body, is one of the leading causes of cancer-related deaths globally. It is now appreciated that metastatic cells take advantage of specific features of surrounding fibrous extracellular matrix that favors invasion. However, the exact contributions of the role of fiber feature size, orientation, and organization remain only partially described. Here using non-electrospinning Spinneret based Tunable Engineered Parameters (STEP) fiber platform, we detail our quantitative findings over the past decade on cancer cell behavior in environments of controlled fiber dimensions, orientation, and hierarchy that can mimic essential features of native ECM. We present a biophysical model of invasion along aligned fibers that starts with cells forming protrusions followed by invasion of cells from a monolayer in single, multi-cell chain and collective modes. Using a mismatch of fiber diameters, we describe a new method to *protrutype* single protrusions and describe migratory behavior of cells in different shapes. Altogether, control over fiber geometry and network architecture enables the STEP platform to unlock a new paradigm in the interrogation of the fundamental biophysical mechanisms underlying the migratory journey of cells during cancer metastasis.

Keywords

Nanofibers · Cancer protrusions · Cancer cell migration · Metastatic invasion · Aligned fibers · Single and collective cell migration · Cell forces · Protrutyping

14.1 Introduction

Cancer metastasis is responsible for 90% of cancer deaths in the United States [1]. Cancer metastasis has been primarily attributed to cancer cells that are able to evade the normal cell-cell junction regulatory system and migrate away from the primary tumor mass, a process often described as epithelial-mesenchymal transition (EMT) [2]. It is well known that during this switch, stable cell-cell junctions and apico-basal polarity are lost, while migratory behavior is enhanced [3, 4]. Upon losing cell-cell contacts, the migratory cells (leader cells) are the pathfinders thought to

A. Mukherjee · A. Jana · B. Koons · A. Nain (✉)
STEP Lab, Department of Mechanical Engineering, Virginia Tech, Blacksburg, VA, USA
e-mail: nain@vt.edu

C. Dong et al. (eds.), *Biomechanics in Oncology*, Advances in Experimental Medicine and Biology 1092, https://doi.org/10.1007/978-3-319-95294-9_14

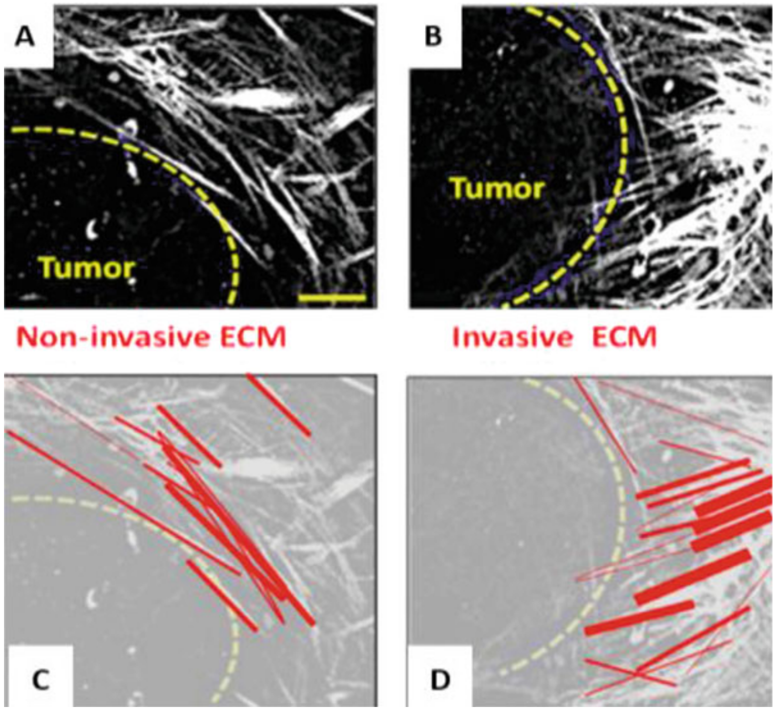

Fig. 14.1 Invasive extracellular matrices (ECM) differ in structure from noninvasive ECMs. Multiphoton second harmonic generation visualization of collagen fibers in mouse tumors of (**a**) noninvasive carcinoma in situ (CIS), a noninvasive early breast carcinoma; (**b**) invasive ductal carcinoma (IDC) with metastases. Scale bar = 50 µm. Note that the presence of metastases is associated with bundled, straightened collagen fibers. (**c**, **d**) The same images as **a** and **b**, with fibers of different widths indicated by different-sized red lines. Image courtesy of Keely Lab (Wisconsin)

be responsible for secreting matrix metalloproteinases (MMP) that cleave the surrounding extracellular matrix (ECM) to make way for the migrating population of follower cells. The leader cells rely on their ability to generate protrusions and exert cellular forces necessary for migration, thus, allowing them to *biophysically* probe the ECM surrounding the tumor. Cancer cells likely take advantage of the aligned fibrous ECM as they have been observed in vivo to move at high speeds for long distances along linear ECM fibers [5–7]. Aligned fiber networks would provide the leader cell with the quickest route through the stroma. Indeed, biopsy samples from breast cancer patients exhibit distinct patterns of perpendicularly aligned collagen fibers, termed tumor-associated collagen signatures (TACS), which are associated with a threefold increased risk of relapse or death for patients [8–11] (Fig. 14.1). Moreover, leader cells obtain extracellular *biochemical* signals from tumor-associated cells including fibroblasts and macrophages that likely contribute to their migratory phenotype [12–14].

Most of what we know in cell migration stems from studies conducted either on 2D flat or in 3D gel environments, with a focus on elucidating the role of elastic modulus of the environment on migration. Through these studies, it is now well known that cell migration is a highly orchestrated cascade of events which starts from sensing the environment through filopodia and then proceeds to cell polarization through formation of stable adhesions in the lamellipodia, followed by translocation of cell body through establishment of actomyosin-based contractile tensional forces [15–17]. At the molecular level, these studies have shown the spatiotemporal localization and importance of small guanosine triphosphate (GTP)-binding proteins (RhoGTPases), Cdc42, Rac1, and RhoA in achieving directed cell migration [17–20]. However, recent studies point to differences between 2D and 3D systems, which result in changes in cell morphology, arrangement of cytoskeleton machinery including RhoGTPases, and altered migratory behavior [21–23]. Adding to the complexity, even within 3D systems, cells exhibit elastic modulus-based distinct modes of migration with non-polarized (lobopodia) and polarized (lamellipodia) cross talk and localization of RhoGTPases [19]. Thus, not surprisingly, in a recent commentary by experts on cell migration [24], it was noted that within the current platforms in practice today, there are generally no accepted methods to cross-validate the findings and compare them with in vivo studies. Furthermore, given the complexity of ECM and limited imaging data available, it has been difficult to achieve a consensus on physiological relevance of in vitro systems, as the experts noted that there are fundamental knowledge gaps in ECM architecture, its properties, and constitutive fibril sizes. However, the experts agreed unanimously upon the need to advance development of more relevant 3D in vitro systems capable of providing cells with accurate and deterministic biophysical fibrillar dimensions, arrangement, and orientations mimicking the native ECM.

14.2 Extracellular Matrix Environment

Cell migration is crucial in developmental, repair, and disease biology [15, 24, 25]. In the context of cancer, it is well appreciated that migration-driven metastasis is more likely to lead to patient death than the primary tumor. Metastasis can represent a very early event in tumor progression, but because micrometastases are not readily imaged due to the complexity of the ECM, the presence of metastases often is not appreciated until much later in the treatment regimen. ECM is a complicated three-dimensional fibrous biopolymer network embedded in a viscous macromolecular gel [26–28], which can be categorized into two major types: the fibrous connective interstitial [7] matrix and the densely packed basement membrane pericellular matrix [29]. In the context of fibrous ECM, fibrillar collagens [30] and elastin have been identified as the major components contributing to ECM tracks. These fibrous proteins are supplemented by a macromolecular network of hydrophilic and acidic components like proteoglycans, hyaluronic acid, etc., which are capable of sequestering water and forming a viscous gel around the fibrous network [30]. The major varieties of the fibrillar collagens include collagen types I, II, III, V, XII, XXIV, and XXVII. Within the ECM, both collagen and elastin exist either as fibrils or fibers, and their structural units are termed tropocollagen and tropoelastin, respectively [31]. In vivo imaging of fibrous ECM using second harmonic generation (SHG), third harmonic generation (THG), multiphoton microscopy, and electron microscopy has revealed a complex hierarchical network of fibers (Table 14.1) [32–36], which is comprised of individual fibers (30–70 nm diameter) that can form bundles (100 nm-microns in diameter) [6, 7, 33, 37–40]. Furthermore, these bundles of fibers can be aligned or seemingly randomly distributed in vivo [11, 16, 21, 41].

14.3 Fiber Manufacturing Techniques

Cells in the native environment have to navigate through stromal (dense and loose connective tissue) and tightly packed basement membrane. The 50–200 nm thick basement membrane surrounds most epithelial cells and vasculature and

Table 14.1 Physical properties of the major classes of ECM fibers

ECM-fiber type	Diameter	Elastic modulus
Collagen fibers	30–100 nm for fibrils [39], 1–20 μm [39] for fibers/fiber bundles	1.2 GPa [42, 43] for mammalian tendon collagen, 100–360 MPa [44] for rat tail collagen type I fibers
Elastin fibers	100–200 nm [39] for fibrils,0.3–2 μm [45] for fibers/fiber bundles	~0.2–1 MPa [43], depending on ECM type
Reticular fibers	20–40 nm [39] fibrils made of collagen mostly	N/A
Fibronectin fibers	10–1000 nm [46–48]	~1 MPa [48, 49]

provides architectural support around which cells attach having basal to apical polarity suggestive of 2D surface. Stromal ECM environment, on the other hand, is composed of nanofibrous natural proteins occurring as small fibrils. Thus, cell interactions on or within ECM can be categorized in two ways: cells stretching over and interacting with the whole mesh, representative of bulk behavior, or cells interacting with the fibrils or bundles of fibers that make up the bulk structure. Therefore, in vitro models mimicking ECM need to account for both the elastic modulus (N/m^2) of the whole mesh and the bending stiffness (N/m) of individual ECM fibrils of varying diameters [50, 51]. In vivo, the tissue architecture varies considerably, and optimal fibrous diameter and pore size result in efficient migration (persistent migration at high speeds). For example, with large number of contacts (low pore size), the cells sense confinement and reduce the migration rate, whereas in environments with large pore sizes, cells make contact with only single fibers, which leads to less cell-fiber contacts causing cells to move more slowly [16, 23, 51–53]. Thus, it is vitally important to engineer in vitro fiber assays to capture cell-fiber interactions and resultant migration in a repeatable and controlled manner.

Since fibrous ECM can be heterogeneous or anisotropic, cells migrating on fibrillar geometries make focal contacts based upon the density and local arrangement of fibers, which leads to altered behaviors [68–76]. Thus, fiber manufacturing platforms need to be capable of depositing fibers hierarchically in multiple layers with repeatable control on diameter, orientation, and interfiber spacing. Furthermore, they should be able to spin fibers of a wide variety of polymers: synthetic, biocompatible, and native proteins. Fortunately, a number of nanofiber manufacturing methods are now available to mimic ECM fibers (Table 14.2).

Of all the reported techniques for biological nanofiber manufacturing, ***electrospinning*** is arguably the most popular process, which allows for the continuous production of fibers ranging from tens of nanometer to a few microns in diameter [77–82]. In this process, polymer solution is pumped through a syringe to a needle where an electrical charge extrudes polymer fibers onto a collecting target [54, 56, 83–85]. With the realization that electrospinning could produce fibers with diameters on the order of those in native tissue, the bioengineering community has seen rapid growth in the use and improvement of electrospinning technique to achieve higher degree of alignment and spatial organization. However, due to the inherent electric instabilities of the electrospinning process, a high degree of parallelism, control on diameter, and the spacing between fibers is difficult to control in multiple layers, which restrict the scope to which cell-fiber interactions can be investigated using electrospinning methods [54, 86–90]. Furthermore, since the jet path of the extruded filament is influenced by the externally applied electric field, the use of multiple nozzles in the same setup has been limited due to mutual Coulombic interactions, resulting in nonuniform nonwoven mats [91–98]. Some of the recent advancements in this respect include far-field electrospinning (FFES) and near-field electrospinning (NFES) [58, 61, 82, 99–CR109]. In FFES, aligned fibers are generated by using a high-speed rotating drum acting as a collector in place of a stationary target [107], wheel-like bobbin collector [99, 109], and patterned electrodes [108] or by modifications to the electric source including using biased AC potentials or an auxiliary counter electrode [82, 100]. On the other hand, NFES has demonstrated improved fiber patterning through reduction of applied voltage and the source-to-target distance [57, 61].

In order to achieve higher consistency and control in fiber diameter and alignment, Brown et al. (2011) [59] introduced the direct write melt electrospinning approach, where instead of electrospinning polymer solutions as performed in conventional electrospinning techniques, polymer melts at elevated temperature (∼70–90 °C) were electrospun. In addition, a significantly lower tip-to-collector distance was used to ensure minimal spread of the extruded polymer fibers. While this approach is able to produce 3D fibrous matrices in various hierarchical architectures with a good degree of fiber alignment, the reported fiber diameters

Table 14.2 Key hallmarks of different fiber spinning techniques

Fabrication method	Major mechanism of fiber fabrication	Diameter range of fibers	Characteristics/advantages	Disadvantages
Conventional electrospinning [54–56]	Electric field (~10–30 kV)	<50–10,000 nm	Mass production of fibers spun from a wide range of polymers.	Presence of a high-voltage electric source results in poor alignment of fibers and widespread in fiber diameters
Near-field electrospinning (NFES) [57, 58]	Electric field (~0.2–1.8 kV)	50–2500 nm	Aligned fibers as compared to conventional electrospinning due to lower electric fields and source-to-target distances involved	Low output compared to conventional electrospinning processes, short source-to-target distance hampers fiber solidification
Direct write melt electrospinning [59, 60]	Electric field coupled with high temperature	10–40 μm	Aligned fiber networks from a wide range of polymers	Very large fiber diameters (~20 μm), thus essentially microfibers, not suitable for mimicking native ECM
Rotary jet spinning [61, 62]	Centrifugal force (up to 75,000 RPM)	425–1600 nm	High throughput of fiber production from a wide range of polymers	Poor control in fiber diameter and restricted to only uniaxial arrays within a ring shaped fiber construct
Pull spinning [63]	Axial/rotational stretch (up to 45,000 RPM)	200–1500 nm	Portable setup and sufficiently high throughput of aligned nanofibers	Poor control over fiber spacing
Direct drawing [64]	Mechanical drawing from solution droplet	50–20,000 nm	Fabrication of aligned arrays of micro-/nanofibers with sufficient precision	Limited to sequential approach and precise silicon tip arrays essential for fiber fabrication and deposition
Spinneret based Tunable Engineered Parameters (STEP) [65–68]	Pseudo dry spinning	<50–10,000 nm	Aligned nanofibers with precisely tunable diameter, spacing, and orientation	Repeatable production of large-diameter (>10 μm) fibers has not yet been investigated using the current version of STEP

are large (typical fiber diameter ~20 μm), and extension to nanofibers remains to be demonstrated.

Since decreasing voltage enhances fiber deposition capabilities, several approaches have removed the electric component entirely. For instance, Badrossamay et al. (2010) [61] demonstrated the rotary jet spinning [110, 111] approach, where, instead of an electric source, centrifugal forces associated with the rotation of a perforated polymer solution reservoir were utilized to extrude polymer nanofibers. Continuous, bead-free nanofibers were obtained at very high rotational speeds (~12,000 RPM) of the perforated reservoir. Pull spinning [112, 113] is another very recent technique demonstrated by Deravi et al., in which devoid of any electric source is able to achieve moderate success in aligning fibers but still lacks control in interfiber spacing. Similar to rotary jet spinning, this approach also utilizes a rotating component for fiber generation. However, instead of an entire rotating perforated reservoir of the polymer solution, a high-speed rotating bristle pulls a polymer droplet into a nanofiber, mainly by the action of the axial stretching forces associated with the bristle rotation. Similarly, another non-electrospinning technique, direct drawing, uses polymer wetted probe tips for precise fiber deposition [64, 114, 115]. Though direct drawing is able to achieve high control on fiber spacing, alignment, and orientation, it remains a sequential technique.

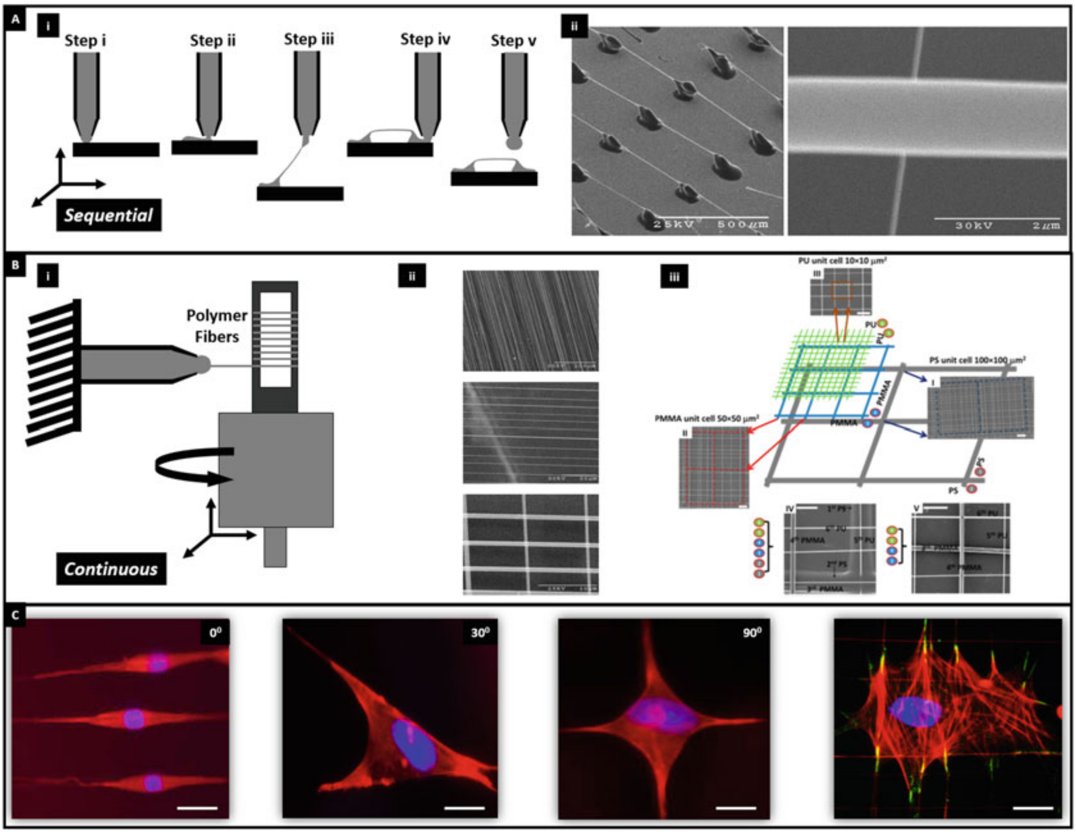

Fig. 14.2 Spinneret based Tunable Engineered Parameters (STEP) fabrication platform**.** (**a**) Sequential method: (i) schematic of fiber formation and (ii) representative SEM images of single- and double-layer fibers of the same and different diameters [116]. (**b**) Continuous high-throughput methods: (i) schematic of fiber formation, (ii) arrays of fibers in single and double layers with varying spacing and orientation, and (iii) hierarchical assembly of a six-layer network of fibers of varying polymers deposited in each layer with varying unit-cell spacing and diameters [66]. (**c**) Achieving control on cell shape with depositing fibers at varying angles in multiple layers. Scale bar is 20 μm

Although some of these novel fiber spinning techniques are capable of producing fiber arrays with a fair degree of alignment, they still lack the ability to control fiber dimensions mimicking a wide range of diameters as observed in native ECM (sub 100 nm-microns) and spatial layouts, which is critical to investigate single- and multicell behavior in a repeatable manner. In this regard, Nain et al. have pioneered Spinneret based Tunable Engineered Parameters (STEP) technique, which does not require the use of an electric source in fiber fabrication process; rather it relies on a physical pull of a single fiber filament from the extruded droplet from a spinneret in both continuous and sequential fiber deposition approaches (Fig. 14.2) [65–68]. For *sequential* approach, single suspended fibers are drawn using a movable probe and fixed-fixed boundary conditions lead to formation of "bridge" structures (Fig. 14.2a) [116]. For *continuous* approach, polymer solution is pumped through a spinneret (probe) and forms a pendent droplet. A rotating substrate contacts the droplet and pulls out solution filaments, which after solvent evaporation and solidification are collected on the substrate in parallel configurations at desired spacing. By depositing fibers on top of each other in multiple layers, hierarchical assemblies of fiber networks with tunable unit-cell dimensions can be created (Fig. 14.2b). Fiber spinning is achieved through a delicate balance of processing parameters (rotating speed, humidity, temperature, etc.) and material parameters (polymer solution concentration, polymer molecular weight, solvent properties), which have direct effects on fiber diameter and morphology [65, 67, 117]. Using both STEP methods (sequential and continuous), fibers in multilayer configurations with a control on diameter, spacing, and orientation can be deposited to precisely control cell shape (Fig. 14.2c).

14.4 Cell-Fiber Interactions

Fibers provide cells with simultaneous 1-, 2-, and 3D mechanistic cues (Fig. 14.3a), as cells align along the fiber axis (1D), stretch between two fibers (2D), and wrap around the fiber by sensing the curvature (3D). Traditionally, electrospun fiber networks have been used to study cell-fiber interactions in the context of developmental biology, specifically investigating the morphology, proliferation, and differentiation of a variety of cell types [118–126]. However, in recent years, electrospun fiber networks have been gaining traction as novel in vitro substrates to mimic the in vivo migratory behavior of tumor cells. In 2014, Nelson et al. [127] demonstrated, using aligned and random electrospun fiber architectures, how fiber alignment can have a significant impact on the motility of the human breast cancer cells (MCF-7, MCF-10A, and MDA-MB-231). Compared to the conventional featureless flat 2D substrates and even randomly oriented fiber networks, cells on aligned fiber architectures demonstrated a significantly higher degree of cell alignment, elongation, and a multifold increase (two to five times) in the migration rate. Interestingly, even in the presence of chemotactic guidance of the chemokine-CXCL12, the breast cancer cell lines demonstrated significant enhancement in migration in aligned fibers as compared to random networks, thus proving that ECM-fiber alignment is one of the key factors driving efficient cell migration. Earlier in 2011, Saha et al. [128] demonstrated cell alignment and spindle-like elongated morphologies of the mouse mammary (H605) tumor cells on electrospun aligned PCL fibers. Interestingly, they reported flat spread-out shapes on their random fiber networks. Apart from metastatic breast cancer, aligned fiber architectures also play a distinctive role in glioma cell migration in vivo, where white-matter tracts provide aligned topographic pathways for efficient and persistent migration. In order to mimic such aligned topography, Rao et al. [72] used aligned electrospun nanofibers to investigate the motility of OSU-2 (glioblastoma multiforme) cells. Here, apart from demonstrating elongated cell shapes on aligned nanofibers, the authors also show how migration rate and focal adhesion dynamics can be significantly altered by varying the stiffness of the nanofibers. Using a three-dimensional aligned and random PCL electrospun fiber scaffolds, Agudelo-Garcia et al. [74] demonstrated that the migration index of U251 glioma cells was significantly enhanced with an increasing level of fiber alignment. Enhancement of U251 glioma cell migration in aligned electrospun PCL fiber networks was also reported by Johnson et al. [129] earlier. In another similar study by Beliveau et al. [130], aligned and random fiber networks were utilized to study the migration of U87MG (glioblastoma multiforme) tumor cells, and it was observed that aligned topography of the electrospun fibers leads to elongated spindle-shaped cells, featuring well-directed and elongated focal adhesions. More recent studies have highlighted the importance of ECM-fiber alignment and anisotropy in metastatic invasion for lesser studied cancers. For example, Alfano et al. [131] used aligned (anisotropic) and random 3D fiber architectures fabricated from electrospinning of PCL solutions, to comprehensively demonstrate that fiber alignment is essential for bladder cancer cell (T24) invasion. Quite surprisingly, in case of random fiber networks, the T24 cells demonstrated little to no binding affinity and invasion capabilities.

While electrospun fiber networks reveal important information on the influence of fibrous topographies on cell morphology, proliferation, growth, differentiation, and more recently in metastatic invasion, it has been

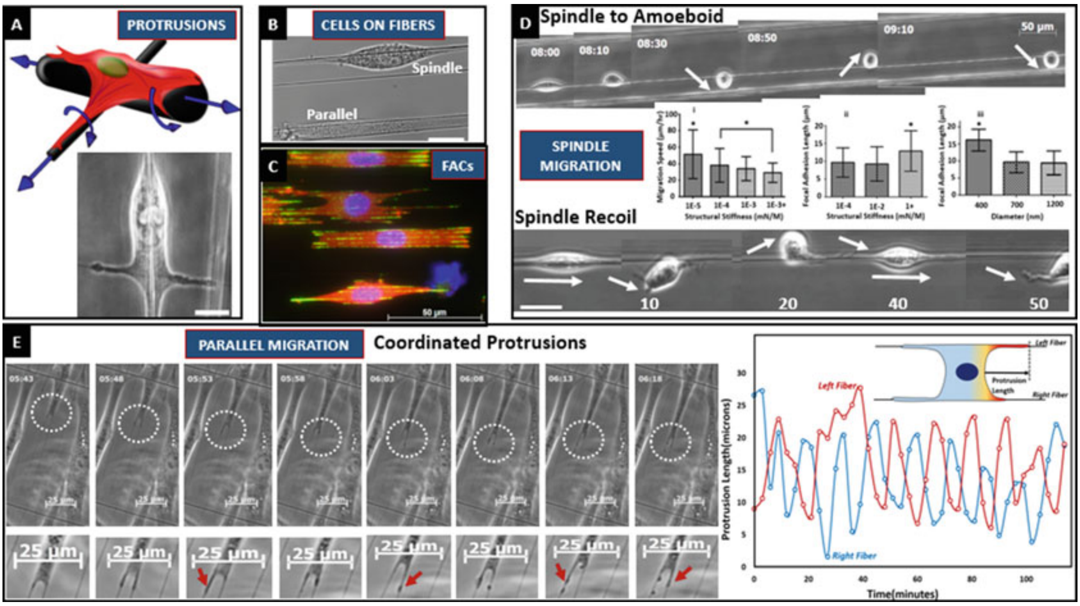

Fig. 14.3 Cell-fiber interactions on different fiber configurations. (**a**) Schematic of protrusion platform with MCF-10A normal breast epithelial cell on large vertical diameter putting two lateral protrusions. (**b**) 3T3 fibroblast attached to single fiber in spindle and to two parallel fibers in parallel morphology. (**c**) Focal adhesion (paxillin: green) clustering occurs at the poles in cells attached to fibers. (**d**) Collage of time-lapse images showing 3T3 fibroblast cell migration on single fiber in spindle shape showing migration (i) switch from spindle to perhaps rounded amoeboid with cell spinning about the fiber axis, shown by arrows, and (ii) in elastic recoil, whereby the cell detaches in a slingshot manner from the trailing edge, reattaches to form spindle again and then slingshots again. Numbers indicate time in minutes. Dashed oval represents time-lapse individual frames, and white line shows the location of leading edge, which remains stationary indicative of contractility built up before slingshot occurs. Inset data showing (i) migration speed decreasing with increasing structural stiffness, (ii) focal adhesion cluster length increasing with structural stiffness, and (iii), at the same structural stiffness, focal adhesion cluster length decreasing with fiber diameter [134]. (Scale bar 25 µm in **b**, **c**, and **d** recoil mode). (**e**) Time-lapse images of mesenchymal stem cell migration in parallel configuration demonstrating synchronous coordinated migration of the left-right protrusions. For each image, the dashed circle is magnified below the respective image, and coordination is shown by red arrow, along with a plot showing coordination between protrusions

challenging to study single- and multicell cell-fiber spatiotemporal interactions in a repeatable manner. The STEP platform (see Table 14.2) offers an alternative method for developing highly aligned, tunable, repeatable nanofiber networks for studying cell-fiber interactions. Since the fibers can be suspended on hollow substrates, this strategy allows the study of cell-fiber interactions exclusively at high spatiotemporal resolutions. For example, using a novel arrangement of crosshatch fibers of contrasting diameters provides the ability to study individual protrusions independent of migration direction [132] (Fig. 14.3a), while using parallel (Fig. 14.3a) or crosshatch fibers in multiple layers allows the study of migratory behavior of single spindle cells (one fiber), parallel cells (two fibers), or polygonal-shaped cells (multiple fibers). Independent of shape on fibers, the focal adhesion sites are mostly clustered at the poles of cells resulting in focal adhesion cluster lengths (FACs, Fig. 14.3c) [76]. However, with increase in fiber diameter, the spatial distribution of focal adhesion sites is distributed along the cell-fiber contact length besides the poles, which allows cells to exert larger adhesion forces [133]. The migratory response of single cells is regulated by both the structural stiffness (bending stiffness) and the fiber diameter, as shown by altered migration rates and focal adhesion cluster lengths (Fig. 14.3d) [134]. Cells typically have higher migration rates with rounded nuclei and smaller adhesion cluster lengths at lower structural stiffness, whereas conversely with increase in structural stiffness, the focal adhesion sites become longer, nuclei become stretched, migration rate decreases, and cells tend to be more persistent in migration toward increasing structural stiffness. Cells migrating in spindle shapes (Fig. 14.3d) can transition into a more rounded *amoeboid* morphology with increased migration rates, or stretched spindle cells migrate with an *elastic recoil* mechanism analogous to release of a stretched rubber band. After recoiling, cells reattach to form spindle shapes and then recoil again from the trailing edge. In the case of parallel migration (Fig. 14.3e), cells stretched between two parallel fibers often display synchronous oscillatory coordination of leading edges during migration [135, 136]. Finally, multicell studies on differentiation have demonstrated a remarkably high efficiency in neuronal differentiation on suspended fibers [137] and, combined with growth factors, controlled differentiation toward muscle tendon and osteoblasts [138].

14.5 Recapitulating Metastatic Invasion Along Fibers

Metastasis is the dissemination of cancer cells from the primary tumor to distant sites where they are able to set up secondary and tertiary colonies [139]. A key step in cancer is the transformation of a healthy microenvironment to a stiffened network of fibrous proteins populated by metastasis-provoking stromal cells. The tumor microenvironment composition consists of a variety of ECM proteins, which provide structural support for migration in the form of fibers, and bundles that vary in size, orientation, and mechanical properties (see Table 14.1). Accumulation of proteins in ECM networks causes tumor stiffness to increase dramatically in certain regions; resections of breast cancer tissue have been measured to be ten times more stiff than its healthy counterpart [140]. In vitro, many studies fail to account for the fact that the increased stiffness is not uniform throughout the tumor; there is a distribution of stiffness magnitudes throughout the tumor's volume modulating cancer cell behavior, and the mismatch of stiffness gradient is more discrete at tumor boundaries [141, 142]. Also, aggregates of stromal cells, such as fibroblasts and macrophages, lay the groundwork for invasion by infesting adjacent areas in order to remodel the ECM for fluent migration as well as secrete stimulating chemical factors that provide directional cues [143]. Besides dispensing chemical signals, these cells are also able to deposit additional ECM fibers, approximately 100–500 nm in diameter, with a wide range of characteristics: dense or sparse, aligned or random, and stiff or compliant [144, 145]. The aforementioned extracellular "jungle" gives testimony to the breadth, depth, and immense complexity of the tumor biophysical microenvironment. Tumor neoplastic growth and dynamic changes in the physical environment provide spatial and temporal cues causing instantaneous cell-ECM interactions leading to metastatic processes [146]. This interaction is composed of, first, the cell extending a protrusion and, second, maturation of the protrusion by recruitment of additional adhesion and cytoskeletal proteins, therefore initiating migration. Subsequently, ECM anisotropy aids invasion by providing a continuous pathway for migration at high speeds without the need for proteolytic ECM degradation [5, 11, 16]. Thus, a simplified "biophysical" model of metastatic invasion along fibers includes two governing phenomena: *sensing and conditioning* followed by *invasion and migration* (Fig. 14.4a). In this model, a single cell or a collection of cells from a tumor mass interfaced with aligned fibers are able to emerge (invade, phase I) along the fiber followed by migration (phase II) away from the tumor. Cells sense the fibers through the formation of filopodia resembling protrusions that mature in cycles of extension and retraction, during which they wrap around the fibers (integrin-based focal adhesion assembly). Over time, the cells preferentially align and move their body outward onto

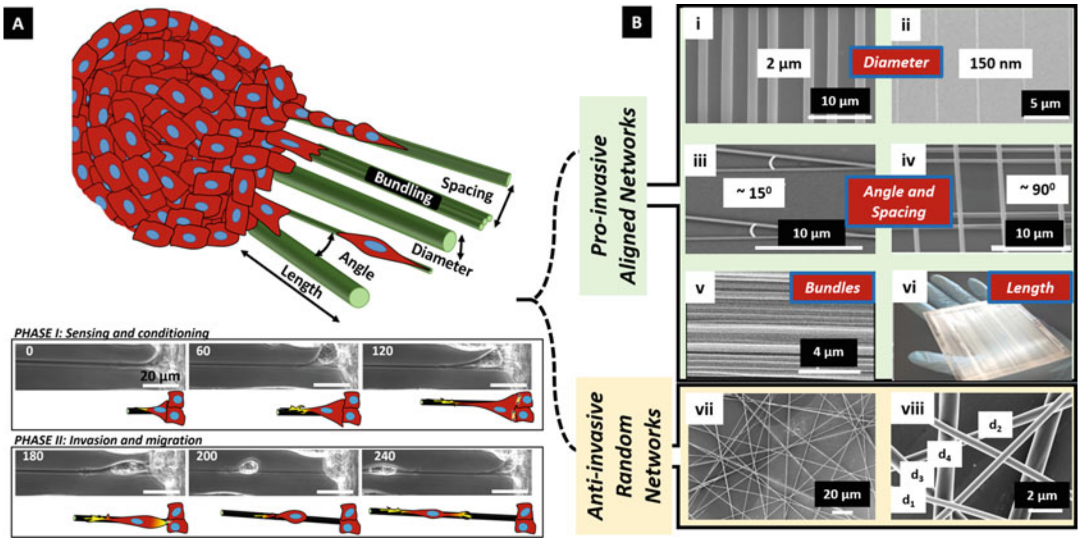

Fig. 14.4 A simplified biophysical model of metastasis along aligned fibers. (**a**) Schematic describing invasion from a tumor mass along aligned fibers and the various parameters needed to describe fibrous ECM environment: length, diameter, spacing, orientation (angle), and fiber bundling. Phase I and phase II show schematic and time-lapse images (breast metastatic MDA-MB-231) of simplified model of invasion (time given in minutes). (**b**) STEP-based recapitulation of fibrous ECM in design of *pro-invasive* networks (i–vi) and *anti-invasive* random networks of varying diameters, spacing, and orientations (vii–viii)

the fiber followed by elongation along the fiber's axis through a conditioning phase of 2–3 h in which they move back and forth on the fiber while maintaining cell-cell junctions at the rear. Subsequently, cells can generate traction forces at the leading edges that are necessary to break the cell-cell contact at the rear, thus allowing them to move away from the tumor mass. Thus, developing a comprehensive understanding of the biophysical regulation of metastatic invasion requires the design of fiber networks with control on fiber diameter, spacing, and orientation to study pro- and anti-invasion conditions at both the single protrusion and single-cell resolution (Fig. 14.4b).

14.5.1 Protrusions on Fibers

Protrusions are projections of cytoplasm from the primary cellular embodiment that perform a specific task, or set of tasks with distinct temporal and morphological characteristics, which also provides aid for force transduction and motility (Fig. 14.5 and Table 14.3) [147–149]. While the importance of protrusions in metastasis is widely acknowledged, their organization and dynamics in 2D and 3D are not fully described [150–156]. Cancer cell protrusions, specifically those that are used to cross basement membranes, have been widely studied using Boyden chambers and degradation assays [157]. These studies have shed light upon the means by which transmembrane protrusions are regulated and affected by cytoskeletal networks, small GTPases, endothelial layer permeability, and oxygen availability [157–160]. Furthermore, these platforms allow investigations of the role of external spatial dimensionality on protrusive behavior. For example, using 2D flat ECM-coated substrates and 3D collagen gels, it was recently demonstrated that protrusions from breast cancer cells of various metastatic capacities can be used to accurately predict invasiveness in 3D environments, while solely observing migration on 2D surfaces was determined to be a poor indicator of 3D migration behavior [161–165].

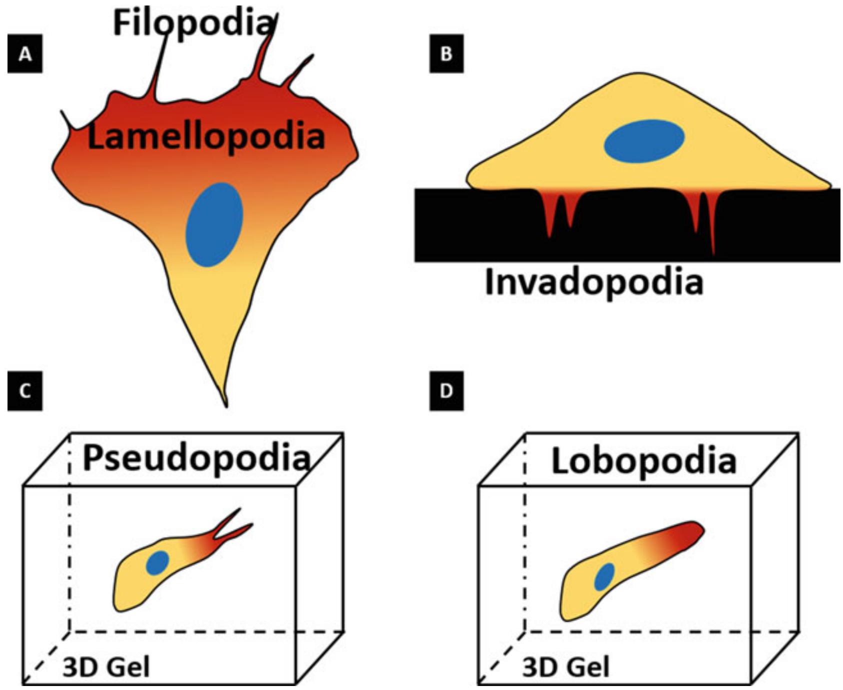

Fig. 14.5 Different types of protrusions (labeled in bold). (**a**) On flat substrate [152]. (**b**) In cancer cells [151]. (**c**, **d**) Cells in 3D gels [174]

Protrusions are typically studied in conjunction with bulk cell body migration. The STEP platform utilizes a suspended crosshatch network of contrasting fiber diameters fused at the intersections to decouple cell body migration from individual protrusions (Fig. 14.6a). Briefly, large-diameter fibers (~2 μm; "base fiber") are deposited orthogonal to smaller-diameter fibers (100 nm to 1 μm; "protrusive fiber") which results in cell migration being arrested along the base fiber axis, while individual protrusions are isolated along the protrusive fibers. In order to quantitate the protrusive dynamics, we defined two morphodynamic metrics: the protrusion length (L) and the protrusion eccentricity (E) (Fig. 14.6a). Protrusion length is defined as the distance from the tip of the protrusion to the projection of the largest ellipse that can be fit along the protrusion curve. The eccentricity is a measure of the morphological curvature of the protrusion where the base and protrusive fibers intersect and is quantified by fitting the largest possible ellipse along the protrusion curve. Lower eccentricities represent "rod-like" protrusions in which the protrusion curvature closely resembles a circle, whereas higher eccentricities represent "kite-shaped" protrusions wherein the curvature of the protrusion deviates significantly from that of a circle. These two metrics can be used in conjunction to characterize the spatiotemporal dynamics of individual protrusions.

Cells attached to the *base* fibers initiate protrusions by first sensing the *protrusive* fibers through the formation of short, rod-like protrusions defined by a low eccentricity value. Subsequently, subject to fiber diameter and ligand availability, the short protrusions can transition (mature) into protrusions of longer lengths at higher eccentricity values before they stabilize on the protrusive fiber (reach a maximum length) and finally retract back to the main cell body. The mechanism of protrusion

Table 14.3 Key characteristics and hallmarks of different types of protrusive structures

Category	Lamellum [152, 163, 166, 167]	Lamellipodia [152, 154, 163, 168, 169]	Filopodia [170–173]	Pseudopodia [174–177]	Podosome [151, 178–180]	Invadopodia [151, 181–183]	Lobopodia [19, 175]
Structure	Broad, "sheetlike" projection; typically seen in 2D substrates		Short, "fingerlike" projection	Long, "fingerlike" projections; typically seen in 3D gels	Actin-rich core, surrounded by signaling proteins		Blunt, cylindrical projection; typically seen in 3D gels
Location	Posterior to the lamellipodia	Leading edge of the cell	Anterior to the lamellipodia	Leading edge of the cell	Ventral surface; behind the leading edge	Ventral surface, clustered under nucleus	Leading edge of the cell
Dimension	Width: ~2–4 μm	Width: ~2–4 μm	Width: 0.1–0.3 μm Length: 3–10 μm	Thinner than lamellipodia; length: >5 μm	Width: 0.5–2 μm Length: 0.5–2 μm	Width: 0.5–2 μm Length: 0.5–2 μm	~5–8 μm
Actin arrangement	Crosslinked and branched	Crosslinked and branched	Parallel bundles	Crosslinked and branched	Branched and unbranched	Branched and unbranched	N/A
Duration	Minutes	Minutes	Minutes	Minutes-hour	Minutes	Hours	N/A

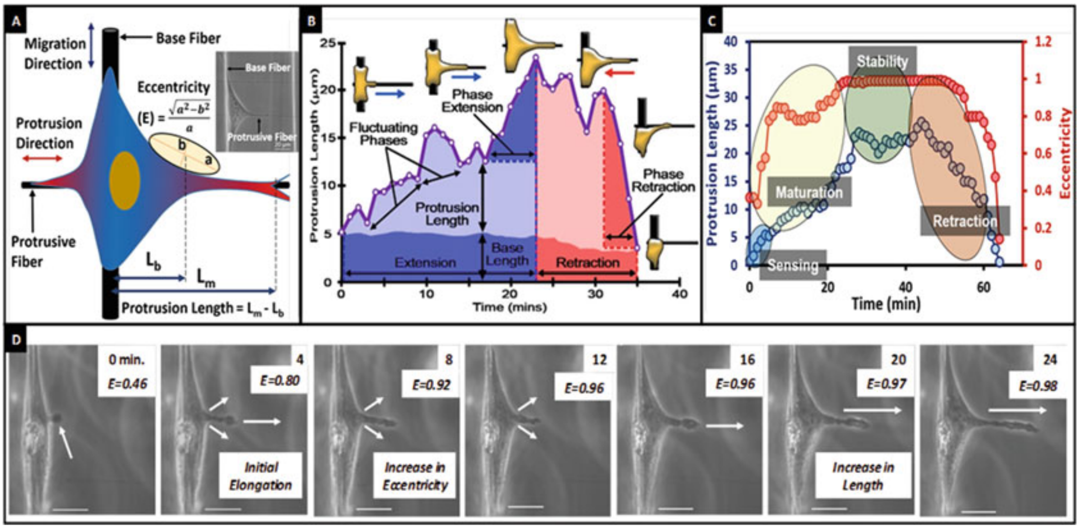

Fig. 14.6 Metrics used to quantify protrusion dynamics. (**a**) A schematic showing the definition of the key parameters used to quantify protrusion dynamics with inset showing an NIH/3T3 cell on the *base* fiber with a protrusion along the *protrusive* fiber. (**b**) Transient profile of protrusion length increase showing different phases in protrusion maturation. (**c**) Transient protrusion profile of a 3T3 cell showing length and eccentricity dynamics during protrusion maturation and retraction. (**d**) Time-lapse images showing the key steps involved in protrusion sensing, growth, and maturation for an MDA-MB-231 cell. Scale bars represent 20 μm

maturation is conserved across fiber diameters and is comprised of a rapid broadening of the protrusion base (increase in E) followed by a growth in the protrusion length via multiple cycles of protrusion extension and retraction (Fig. 14.6b–d). Fiber curvature dictates the dynamics of the protrusion maturation process with protrusions typically reaching eccentricities of 0.95 and higher significantly faster on flat protrusive ribbons of equivalent width (πD) compared to round fibers (Fig. 14.7 shown by arrows). This result suggests that compared to high curvature round fibers, protrusions on low curvature flat ribbons mature faster and more deterministically. Thus, while flat fibers ubiquitously generate broad mature protrusive behavior, they are unable to capture the sensitivity of high curvature ECM-mimicking fibers.

This platform can be further extended to distinguish between the protrusive dynamics of different cell lines ("protrutyping"). In addition to looking at the role of fiber diameters, the platform can also be used to interrogate if fibronectin coating on fibers in varying concentrations (2, 4, and 16 μg/ml) affects protrusive behavior. Fibronectin is a major ECM glycoprotein that plays an important role in promoting cell adhesion to the surrounding substrate and is native to both neural and breast tissues [184–186]. Additionally, fibronectin has previously shown to play an active role in inducing epithelial-mesenchymal transition such that increased fibronectin levels have been implicated in facilitating tumorigenesis in breast tumors [187]. Thus, by varying both the fiber diameter and ligand density, the STEP platform is able to partially capture the heterogeneity associated with tumor microenvironments and its influence on cancer cell protrusive dynamics. Protrutyping the protrusive dynamics between two breast cancer cell variants reveals that the more metastatic breast adenocarcinoma MDA-MB-231 puts out significantly longer protrusions in comparison with the relatively less metastatic normal breast epithelial MCF-10A (Fig. 14.8). This result suggests that the protrusion length could be indicative of the metastatic potential of a cell. Furthermore, the

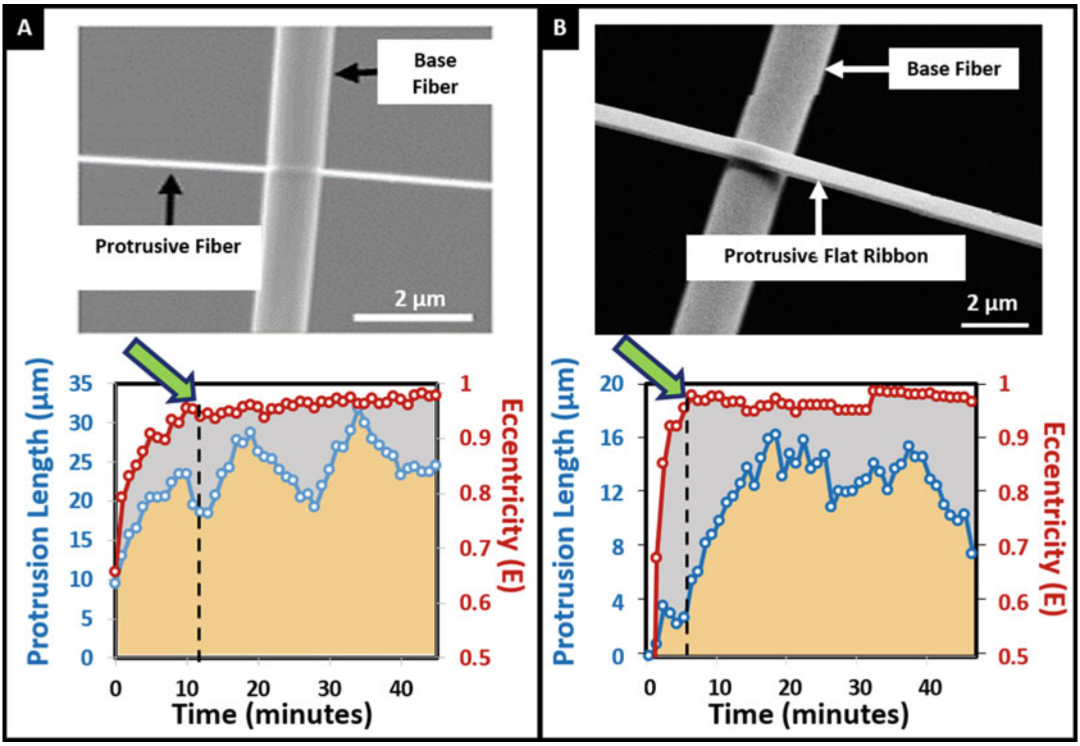

Fig. 14.7 Characteristic protrusion profiles. SEM images of (**a**) round protrusive fiber and (**b**) flat protrusive ribbon. Representative transient protrusion profiles seen on (**c**) round protrusive fiber and (**d**) flat protrusive ribbon. Arrows indicate that on flat ribbons, high eccentricity is achieved significantly faster compared to round fibers

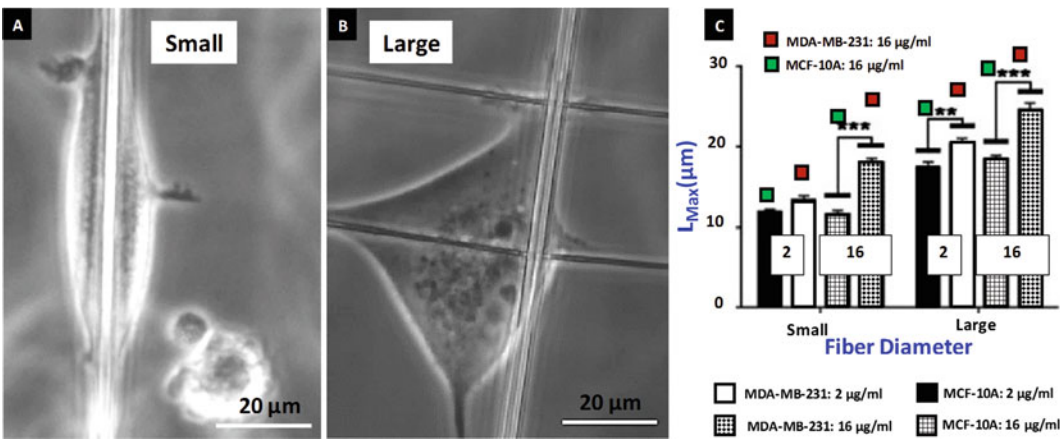

Fig. 14.8 Differentiating between MDA-MB-231 and MCF-10 protrusion dynamics using protrusion metrics. Phase images show MCF-10A protrusions on (**a**) small and (**b**) large diameter protrusive fibers. (**c**) Bar graph shows the protrusion length comparison between less metastatic MCF-10A and relatively more metastatic MDA-MB-231 (N = 100 protrusions per category). *** denotes $p<0.001$, ** denotes $p<0.01$, * denotes $p<0.05$. Adapted from Koons, et al. [132]

platform can be used to *protrutype* highly invasive cell lines having different lineages. The analysis between MDA-MB-231 and DBTRG-05MG cells shows breast cells to exhibit strong dependence on fiber diameter and ligand concentration compared to brain glioblastoma DBTRG-05MG (Fig. 14.9). Altogether, quantitating single protrusions on ECM-mimicking fibers demonstrates that protrusive behavior is highly sensitive to fiber geometry, which (1) flat ribbons cannot capture, and (2) is cell specific.

The contrasting curvature platform can be used to interrogate the organization and localization of cytoskeletal components inside individual protrusions (Fig. 14.10). The long lengths and broad morphologies achieved by protrusions are indicative of f-actin to be present in protrusions across the entire spectrum of eccentricity values associated with the protrusive cycle. Similarly, tubulin is also present at all eccentricity values albeit occurring with relatively lower probability (∼20–60%) at low eccentricities and higher probability (∼75–100%) at high eccentricities. In contrast to f-actin and tubulin, both of which localize across the entire range of eccentricity values, major vimentin fronts are rarely detected in protrusions of eccentricity lower than 0.8. This suggests that the protrusion base needs to broaden out significantly prior to the introduction of vimentin into the protrusions, thus indicating a diminished role of vimentin in protrusion initiation and maturation.

14.5.2 Cell Invasion Along Fibers

After using protrusive structures to actively probe the surrounding, the next step for a cell during metastasis is directed migration toward the blood vessels [188]. To study *invasion* and *migration*, cell monolayers can be interfaced with suspended fibers (Figs. 14.11 and 14.12). In doing so, cells at the edge of the monolayer sense the fibers through formation of protrusions followed by cells emerging (invading) from the monolayer onto the suspended fibers [189]. Since metastatic invasion occurs as single or collection of *leader* cells, the diameter and spatial layout of fibers allow us to capture these invasive modes in vitro. *Leader* cells emerge on the fiber networks in three distinct modes: *recoil and chain* on single fibers and *collective* (multiple chains) on multiple fibers. *Recoil* mode signifies a single cell abruptly detaching from the monolayer and recoiling away analogous to the release of a stretched rubber band. This primarily occurs when the cell body is aligned at an angle with the fiber axis. *Recoiling cells* have higher detachment speeds that enable them to advance longer distances away from the monolayer. However, they can switch directions and return to the monolayer, thus having an overall lower persistence. In contrast, when the cell body is symmetrically aligned with the fiber axis, a collection of few cells with intact cell-cell junctions are observed to emerge from the monolayer. On densely packed fibers, multiple chains emerge simultaneously as large collective groups. Fiber diameter also plays a role in emergence as a higher tendency for the recoil mode of emergence was observed on the 300 nm and 500 nm diameter fibers, while on the 1000 nm diameter fibers both the recoil and chain emergence modes had a similar probability of occurrence. Furthermore, the speed of detachment in *recoil* mode is dependent upon fiber diameter (250 ± 15, 425 ± 14, and 400 ± 30 μm/h on 300 nm, 500 nm, and 1000 nm diameter fibers, respectively). This can be explained by the organization of focal adhesions on fibers of varying diameters (Fig. 14.13). Cells attached to fibers form focal adhesions primarily at the poles on smaller diameter fibers and along the entire cell body-fiber length on larger diameter fibers. The arrangement of these adhesion sites leads to stronger cell-fiber adhesion forces on large diameter fibers, thus perhaps leading to reduced *recoil* invasion mode on large diameter fibers [134].

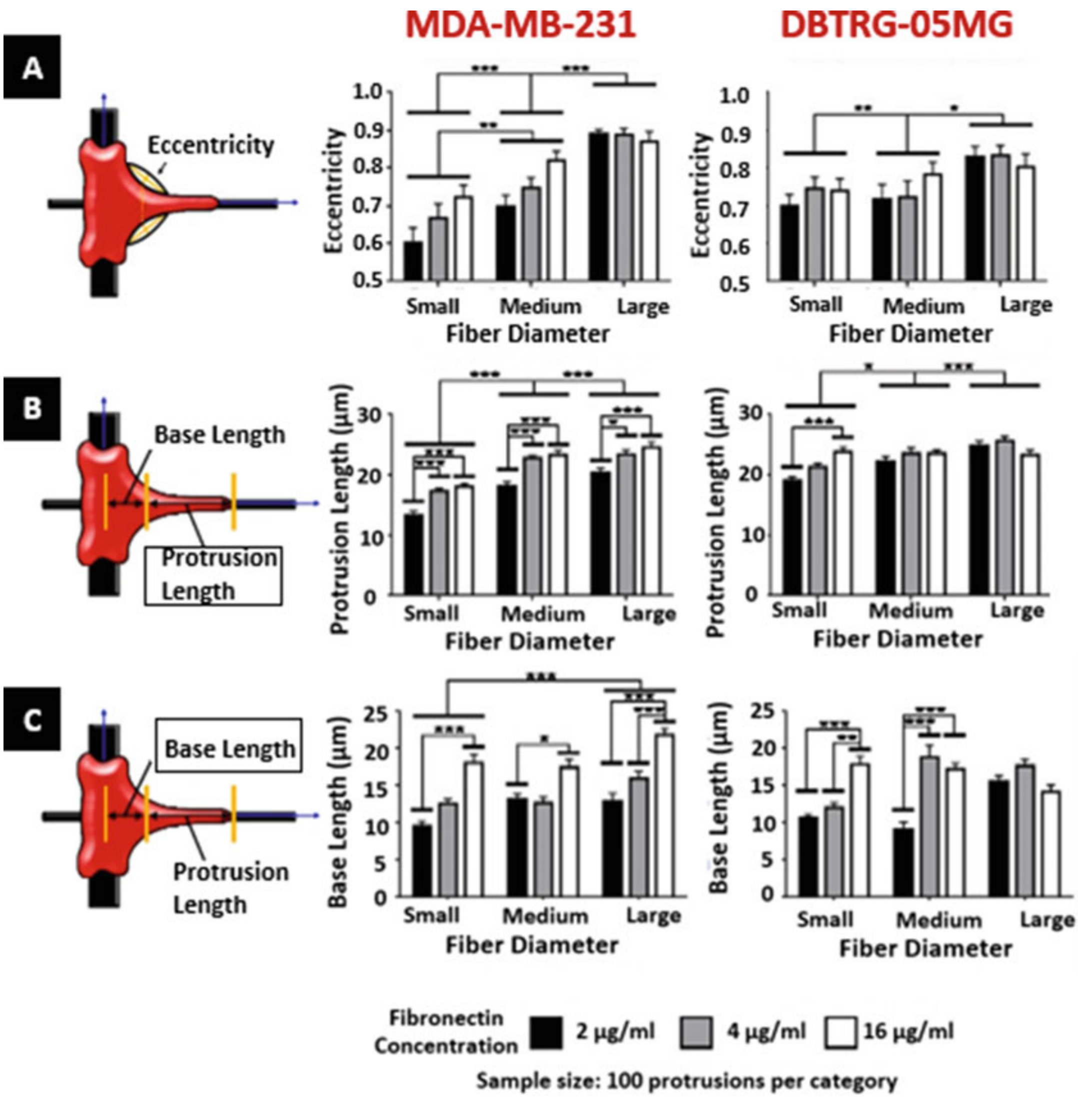

Fig. 14.9 Differentiating between MDA-MB-231 and DBTRG-05MG cell lines using protrusion metrics. (**a**) Eccentricity increases with fiber diameter, but no statistically significant differences were found due to fibronectin concentration ($n = 30$ per test category). (**b**) Maximum protrusion length and (**c**) base length metrics reveal that MDA-MB-231 cells modulate their protrusion lengths as a function of both the fiber diameter and fibronectin coating compared to DBTRG-05MG ($n = 100$ per case). *** denotes $p < 0.001$, ** denotes $p < 0.01$, and * denotes $p < 0.05$. Adapted from Koons, et al. [132]

14.5.3 Cell Migration on Fibers

Post-invasion, cell migration on fibers occurs in either single or collective mode. Migration speed for single cells is dependent upon the number of contacts the cell makes with fibers. Cells on suspended parallel nanofibers, with spacing larger than 20 µm, typically assume a "spindle" shape and interact only with the single fiber as they migrate. Conversely, for nanofibers with spacing smaller than 20 µm, the cells spread between the two parallel fibers. When the cells reach a fiber junction, they typically take up a "polygonal" shape (Fig. 14.14). Compared with flat and 2D substrates, myoblast C2C12 cells on suspended fibers have the ability to almost double their mi-

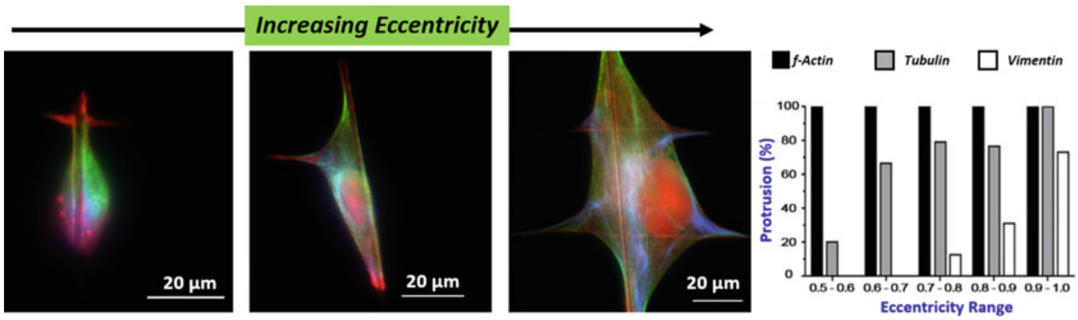

Fig. 14.10 Key cytoskeletal components in protrusions. Immunofluorescent imaging shows the distribution of f-actin (red), tubulin (green), and vimentin (blue) localization in cells with increasing intensity along with quantitation showing that vimentin localizes in individual protrusions at high eccentricities

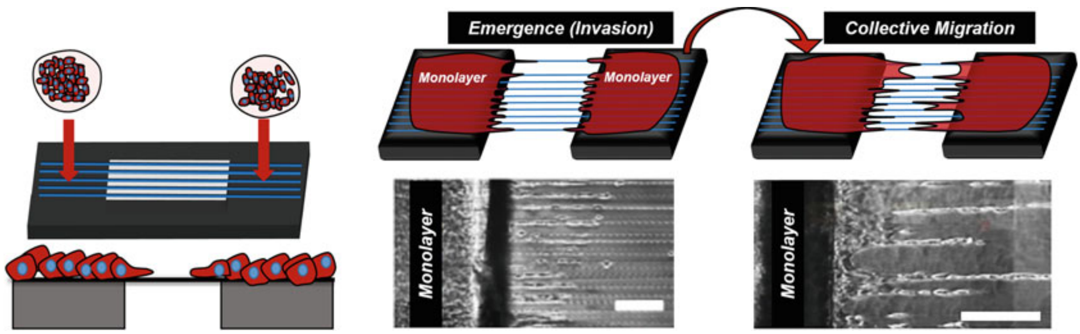

Fig. 14.11 STEP-based nanofiber platform to study cell invasion and collective migration. Schematic and phase contrast images show the application of the STEP platform to study cell invasion and collective cell migration. All scale bars are 20 μm. Adapted from Sharma et al. [189]

gration rate due to enhanced FAC alignment and polarization of contractile forces (Fig. 14.14). It is also interesting to observe that even under the administration of drugs that are well known to impact FAC dynamics such as blebbistatin (inhibits myosin contractility), nocodazole (inhibits microtubule polymerization), and cytochalasin-D (disrupts actin filament formation), the migration rate of cells on fibers is still greater than their counterparts on flat substrate [76]. Overall, spindle cells have highest migration rate compared with the other three categories but tend to exhibit lower persistence. Highly aggressive cancerous brain glioblastomas (DBTRG-05MG) also exhibit similar behavior in single-cell migration with spindle shapes having faster speeds compared to their counterparts on flat 2D substrates and on suspended crosshatch pattern of fibers (Fig. 14.15a). In addition, Estabridis et al. [190] investigated the migration of U251 glioblastoma cells in precisely aligned 1D and 2D crosshatched nanofiber arrays, and it was revealed that the glioblastoma cells assumed spindle morphologies in the aligned 1D arrays and exhibited faster and more persistent migration, as compared to the 2D crosshatch networks. A comprehensive analysis of spindle cell migration reveals that cells modulate their migratory response to both fiber diameter and structural stiffness (bending stiffness) of the suspended fibers [38, 76, 134]. Structural stiffness accounts for the length, diameter, and material stiffness (Young's modulus and measured in units of N/m^2) and thus is another property to study cell behavior on fibers, as it scales with both fiber diameter and length$\left(\sim \frac{\text{Diameter}^4}{\text{Length}^3}\right)$. As the cell spreads and migrates along a single suspended nanofiber, the migration rate and nucleus shape index decrease with increase in structural stiffness, while the

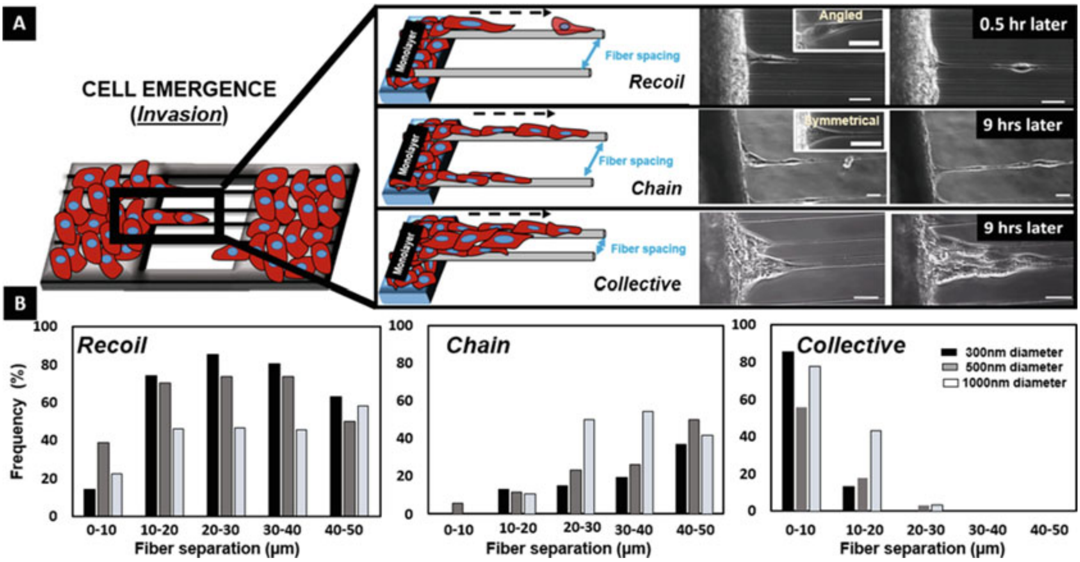

Fig. 14.12 Invasion of leader cells. (**a**) Schematics and phase contrast images showing leader cells leaving the monolayer in three distinct emergent modes: *recoil*, *chain*, and *collective* (multichain) groups. (**b**) Occurrence frequency of the three distinct modes of emergence on fibers of different diameters. Percentages have been calculated for each diameter and fiber spacing. For instance, on 300 nm diameter fibers with <10 µm spacing, about 14% emerged as *recoils*, none as *chains*, and about 86% as multichain *collective* groups. All scale bars are 25 µm. Image from Sharma, et al. [189]

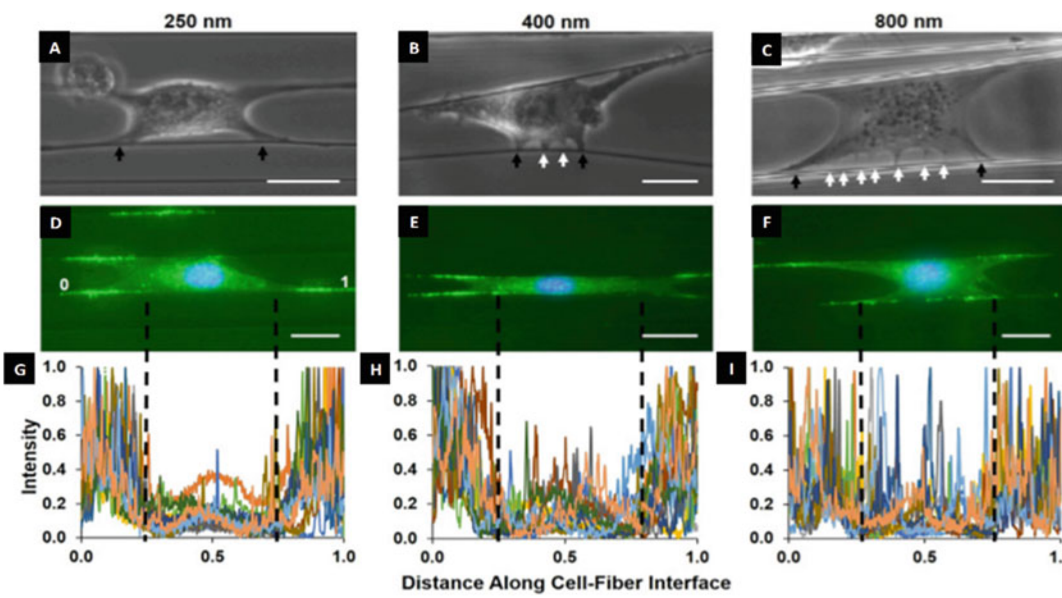

Fig. 14.13 Focal cluster distribution along the cell-fiber interface as a function of the fiber diameter. (**a**–**c**) Phase images of cells being pulled by a probe on 250-, 400-, and 800-nm-diameter fibers, respectively. The two primary peripheral clusters (black arrows) are shown distinctly from intermediary groups (white arrows), which increase with increasing diameter. (**d**–**f**) Fluorescence images showing paxillin signal presence along the cell-fiber axis. (**g**–**i**) Corresponding intensity of the paxillin signal with primary cluster zones separated from intermediary zones by black dashed lines. As fiber diameter increases, signal intensity within this region increases. Scale bars represent 25 µm. $N = 42$. Image from Sheets et al., 2016 [133]

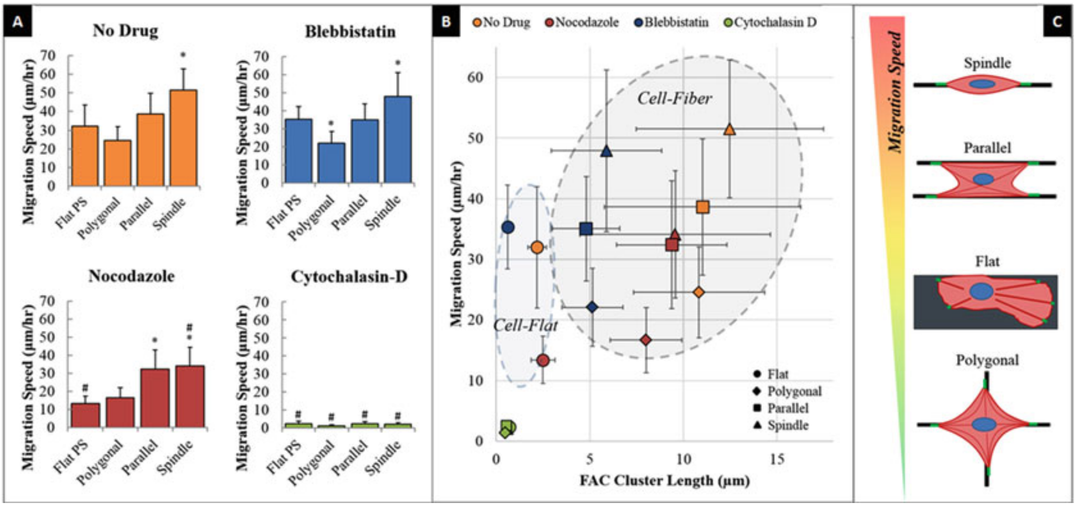

Fig. 14.14 Cell migration speed as a function of the cell shape and drug influence. (**a**) Impact of three different drugs on migration speed. (**b**) Migration speed as a function of the focal adhesion complex (FAC) cluster length for four different cell configurations on STEP nanofiber platform. (**c**) Schematic of three different shapes for cells on suspended fibers. Image from Sheets et al., 2013 [76]

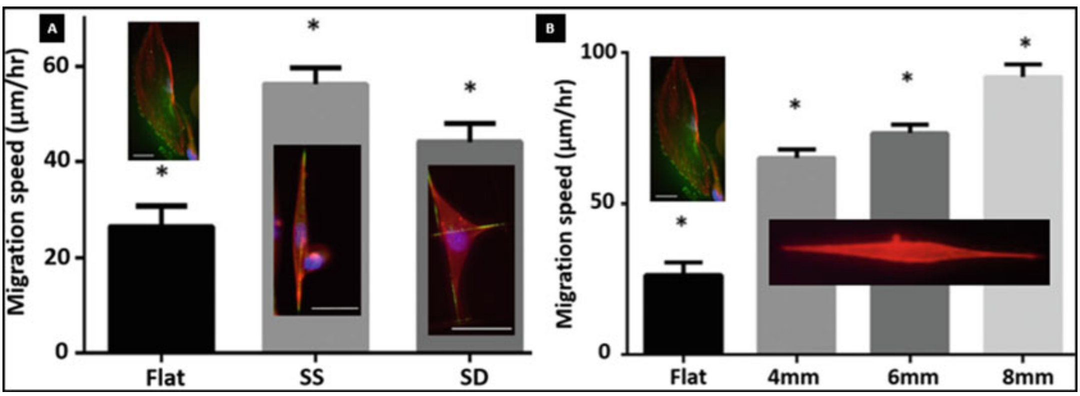

Fig. 14.15 DBTRG-05MG migration dynamics on suspended fibers. (**a**) Migration speed was evaluated on flat substrate ($N = 14$), single suspended nanofibers (SS, $N = 56$), and double suspended nanofibers (orthogonal, SD, $N = 62$). A statistical difference was observed between the migration rates on flat, SS, and SD nanofibers (student's t-test, $p = 0.0004$ for SS-flat, $p = 0.0294$ for SD-flat, and $p = 0.0171$ for SS-SD). The inset shows fluorescent images of cells on the three substrates analyzed. Scale bars represent 50 µm. (**b**) Cell migration was evaluated on SS fibers of lengths 10 mm ($N = 60$), 6 mm ($N = 101$), and 4 mm ($N = 120$) and compared to flat ($N = 14$). Significant difference in migration rate was observed across all the fiber lengths tested (student's t-test, $p < 0.0001$ for 10 mm-flat, 10–4 mm, 6 mm-flat, 4 mm-flat; $p = 0.0001$ for 10–6 mm; and $p = 0.0439$ for 6–4 mm)

focal adhesion cluster lengths (FACs) increase. At similar structural stiffness values, migration rates increase, and FACs decrease with increasing diameter [38, 134]. Our previous studies have shown that cell migration increases with decreasing bending stiffness for single glioblastoma (Fig. 14.15b). Thus, the invasion mode and kinetics of single-cell migration are sensitive to fiber (1) diameter, (2) spacing, and (3) structural stiffness.

Post-invasion, collective cell migration occurs through formation of cellular bundles termed *cell streams* (Fig. 14.16a), which initially exhibit a fast advancement rate (~200 µm/day).

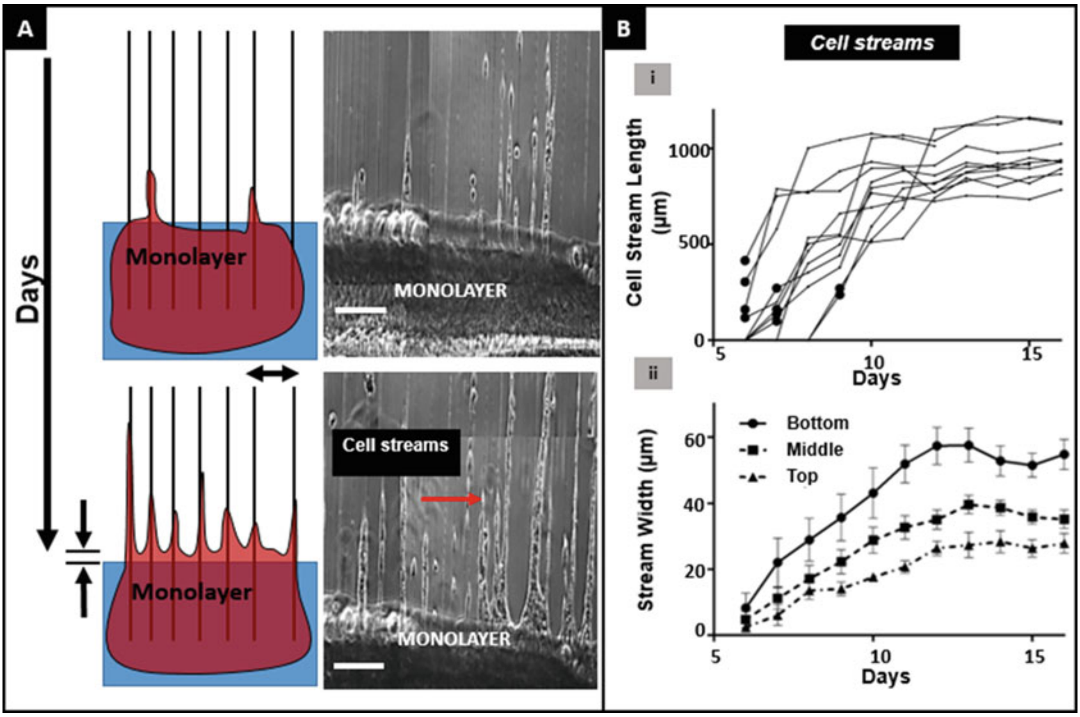

Fig. 14.16 Collective cell migration on STEP nanofibers. (**a**) Representative schematics and time-lapse images of *cell stream* advancement over time. Scale bars are 200 µm. (**b**) (i) Kinetics of *cell stream* ($n = 10$) advancement. The black dots represent the instances when the *cell stream* length exceeded 100 µm. (ii) Average *cell stream* ($n = 10$) width measured at three locations: top, middle, and bottom of the *cell streams* over days. Adapted from Sharma et al. [189]

Interestingly, the migratory rates of highly proliferative in vivo migratory tongues typically found in early stages of wound repair (150–300 µm/day [191–193]). The width of individual *cell streams* (measured at the base, middle, and tip of streams) increases and saturates (Fig. 14.16b(ii)). Collective *cell stream* migration occurs in a highly persistent manner with advancement away from the monolayer. Occasionally, single or a few cells detach from the tip of the *cell streams*, which further contributes to advancement away from the monolayer.

14.5.4 Plasticity in Cell Migration on Fibers

Migrating cells have to squeeze, push, and tug through the complex ECM to achieve efficient migration (persistent over long distances). Cells achieve this by adapting to the changes in local microenvironment by shifting their migratory modes in a process commonly referred to as *plasticity*. Cells migrating in *mesenchymal* mode typically have a well-defined integrin-based lamellipodia resulting in elongated spindle-like morphology (fibroblast-like morphology) [194]. In 3D matrices, mesenchymal migration occurs with the additional step of ECM degradation (proteolysis) [195] and can lead to elastic modulus-based non-polarized (lobopodia) and polarized (lamellipodia) cross talk and localization of RhoGTPases [19]. In contrast to *mesenchymal* migration, many established tumor cell lines show an *amoeboid* migration which is characterized by a rounded or “balled-up” morphology and an integrin-independent motility [196]. These cells typically show efficient and rapid alternating cycles of cytoskeletal expansion and contraction in addition to a very high

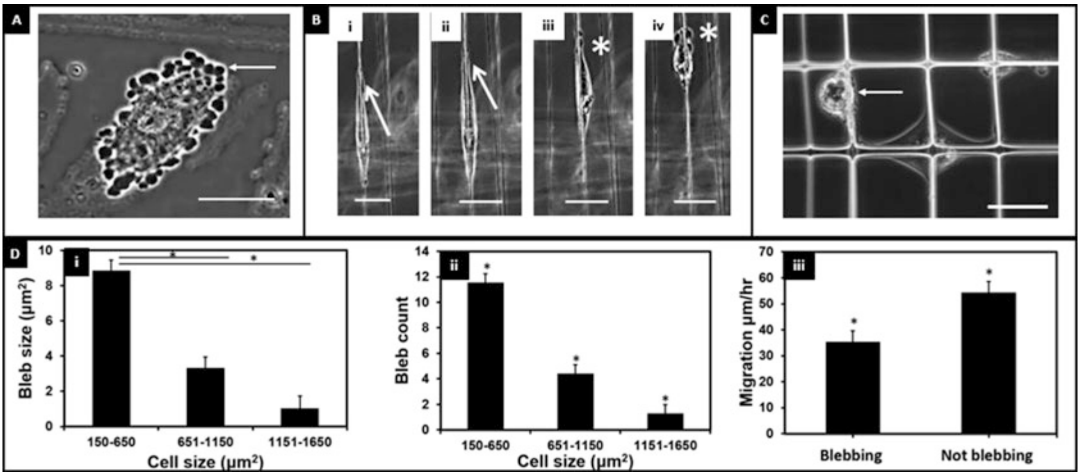

Fig. 14.17 DBTRG-05MG blebbing dynamics on suspended fibers. Migration (**a**) continuous blebbing behavior of DBTRG-05MG on flat substrate. Scale bar represents 20 μm. (**b**) Time-lapse image of DBTRG-05MG migrating along a single suspended nanofiber at 10-minute intervals. We observe that the cell only starts blebbing (denoted by *) when the cell spread area has reduced considerably. Scale bar represents 50 μm. (**c**) DBTRG-05MG which has sufficient cell spread area does not show signs of blebbing, while the cell with the reduced spread area shows blebbing (denoted by white arrowhead). Scale bar is 50 μm (**d**.i and **d**.ii) bleb size and bleb count as functions of cell spread area for DBTRG-05MG cells. Bleb size for cells with spread area of 150–650 mm^2 ($N = 109$) was significantly higher than those for areas 651–1150 mm^2 ($N = 80$) and 1151–1650 mm^2 ($N = 36$) (student's t-test, both $p < 0.01$). Bleb size for a cell spread area of 651–1150 mm^2 was almost significantly higher than those for areas 1151–1650 mm^2 (student's t-test, $p = 0.05$). (**d**.iii) Migration rate for DBTRG-05MG cells showing blebbing dynamics ($N = 31$) was significantly lower than cells not showing blebbing ($N = 30$) ($p = 0.002$). Figures adapted from Sharma et al., 2013 [38]

degree of plasticity that allows the cells to "squeeze" through small pores in the ECM [197–199]. *Mesenchymal* mode of migration relying on engagement of integrins is thus slower than the *amoeboid* mode. Metastatic cells often display another type of protrusive structure known as *blebs*. Long considered the hallmark of apoptosis, *blebs* lead to changes in nuclear shapes, mitotic disturbances causing genetic instability, multidrug resistance in tumor cells, invasiveness, ability to escape apoptosis, and motility [17, 19, 200–202]. Blebs are hydrostatic pressure-driven protrusions that appear as spherical (Fig. 14.17a shown by white arrow), highly dynamic extensions from the cell body [203]. These structures are primarily observed in cells undergoing 3D migration (and in some cases on 2D substrates as well) [200]. In contrast to actin polymerization-driven formation of lamellipodia and filopodia, bleb formation is hypothesized to be due to a rupture or local decrease in the membrane-cortex attachment, thus leading to a rapid increase in hydrostatic pressure [200, 202, 203]. Interestingly, studies have also shown that some cells are capable of switching from bleb formation to more traditional protrusive structures in response to the topographical properties and intracellular signaling [16, 204]. Single glioma cells migrating in spindle shapes on suspended fibers also display *plasticity* in migratory modes by switching from elongated shapes to rounded cells with well-defined *blebs* as protrusive elements (Fig. 14.17b). Further, the same cells migrating on crosshatch pattern of fibers stretched between intersecting fibers have no to minimal *blebs*, whereas those attached to single fibers display *blebs*. In fact, blebbing dynamics scales with area as larger *mesenchymal* cells have smaller and less number of *blebs* resulting in higher migration speeds (Fig. 14.17c).

14.6 Future Outlook

ECM-mimicking suspended nanofiber platforms offer integrative and multiscale abilities to study key biophysical phenomena in metastatic invasion: protrusions, invasion, and migration. We have developed a reductionist model of metastatic invasion using ECM-mimicking suspended and aligned fiber architectures. To describe invasion in detail, our model in future will need to include multiple layers of sophistication to include ECM porosity through deposition of multiple layers of fibers, stromal interactions, and appropriatechemical cues. Cells in their native environment are always exerting or withstanding forces. Currently, there is incomplete knowledge in force-driven invasion of cells in stiffer environments found around tumors [71, 205–208]. In this regard, we have pioneered fused-fiber nanonet-based *Nanonet Force Microscopy* (*NFM*) to measure single- and cell-cell forces and shown single-cell sensitivity to drug response (Fig. 14.18a). NFM can also be used to measure the forces exerted by single protrusions (Fig. 14.18b) during the process of maturation for both stationary and migratory cells. Furthermore, NFM can be used to measure cell-fiber adhesion forces using

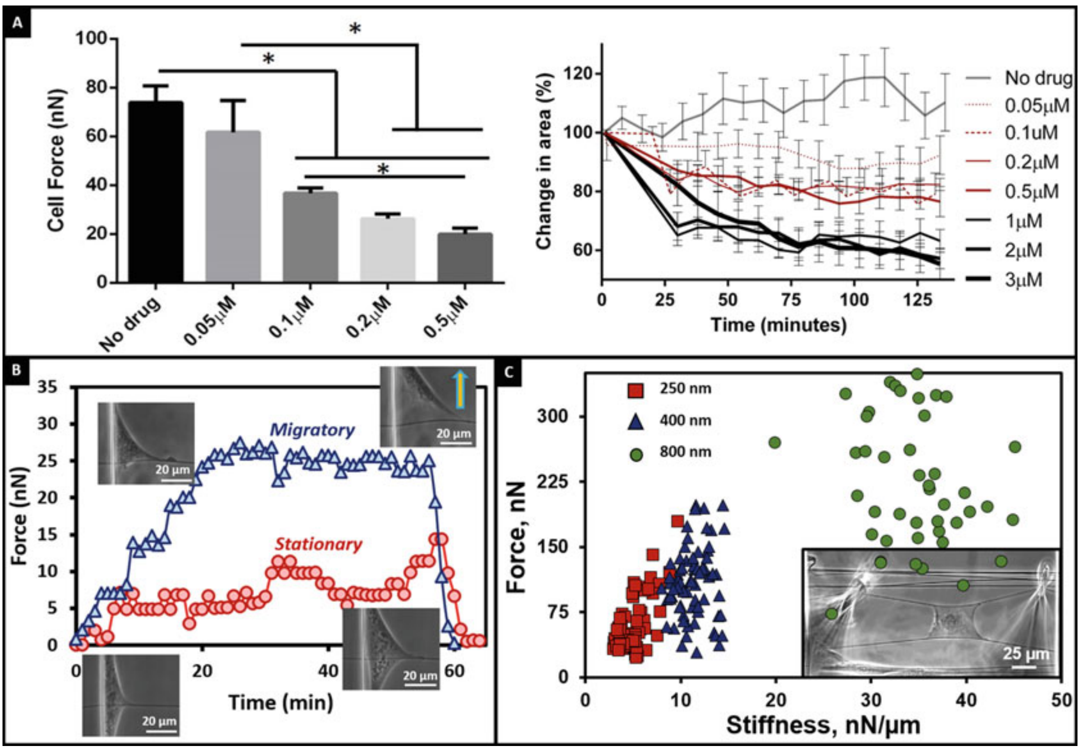

Fig. 14.18 Measuring single-cell and individual protrusion forces using NFM. (**a**) Average contractile forces exerted by single DBTRG-05MG cells without and with 0.05 μM ($N = 116$ and 10, respectively), 0.1 μM ($N = 45$), 0.2 μM ($N = 63$), and 0.5 μM ($N = 49$) cytochalasin D exposure. Forces reported were measured after 30 min exposure to the drug. Error bars represent the standard errors. Also shown in right panel are the temporal dynamics of cell spread area of single DBTRG-05MG with (0.05, 0.1, 0.2, 0.5, 1, 2, and 3 μM) and without exposure to cytochalasin D. (**b**) Representative profiles of transient force dynamics of protrusions put out by two NIH/3T3 fibroblasts in stationary and migratory modes. Migrating cells exert higher forces (direction of migration is shown by arrow), and inset includes representative phase contrast images of both cells at 15 and 50 min. (**c**) The role of structural stiffness in regulating cell-substrate forces. Inset shows phase image of C2C12 cell responding to an externally applied force. Panels **a** and **c** are adapted from Sharma et al. [219] and Sheets et al. (2016) [133], respectively

external manipulation (Fig. 14.18c). Altogether, the ability to measure single-cell and multicell forces using ECM-mimicking fibers provides new abilities to calibrate normal cell behavior and interrogate disease onset, progression, and therapeutic response.

Cell migration requires establishment of polarity (front to back) and precisely architected cytoskeletal arrangement, adhesion organization, and formation of filopodia and lamellipodia. These depend upon the differential activity of small guanosine triphosphate (GTP)-binding proteins (RhoGTPases) signaling of small molecules Cdc42, Rac1, and RhoA [18–20, 25, 209, 210]. Most of what we know in this signaling comes from studies conducted on flat substrates, which have demonstrated that Cdc42 is active toward the front of the cell and inhibition or activation of Cdc42 can disrupt directionality in migration [18, 25]. One direct consequence of Cdc42 localization is activation of Rac1. Activation of both these proteins mediates actin polymerization in protrusions in the direction of migration. The rear of the cell is defined by the activity of RhoA. Activation of Rac1 at the front of the cell suppresses Rho and myosin activity, whereas Rho is more active at the rear and sides of cell where it suppresses Rac1, which in turn tends to keep the formation of protrusions in the direction of migration at the front of the cell. Rho contributes to actomyosin contractility through its effecter Rho kinase (ROCK), which allows for buildup of tensile stresses inside the cell body through formation of f-actin stress fibers. An interesting and recent development in the field has been the demonstration that cells in 3D do not require polarized patterns of RhoGTPases to achieve efficient migration (higher motility rates and increased persistence). Furthermore, cells are observed to shift their migration modes (plasticity) in response to changes in elasticity of the environment with distinctly different organization of Rho family members [16, 19, 24, 211, 212]. Thus, even the familiar class of RhoGTPase family of molecules for which we know almost everything on 2D is regulated and utilized differentially in 1- and 3D. The mechanisms driving the spatiotemporal regulation of these molecules in cells attached to fibers of varying curvatures and the associated force signatures are to the best of our knowledge nonexistent. A key challenge to elucidate these mechanisms lies in the inability to image cell-fiber interactions on fibers of high curvature. It is clear that focal adhesion clusters spatially organize differentially on fibers of varying diameters, with longer FACs on smaller diameter fibers, suggesting an area conservation along the fiber axis. However, it is unclear if the integrin-driven focal adhesion assembly is altered, as cells have lower cell-fiber adhesion forces on smaller diameter fibers (Fig. 14.18c).

Metastatic invasion in-vivo occurs in the presence of both biophysical and biochemical gradients [188]. In recent years, microfluidic devices have advanced significantly to allow long-term establishment of chemical gradients [213–216] and sophisticated invasion models. Recently, Kamm and colleagues have used 3D microfluidic assays to investigate the role of monocytes in cancer cell extravasation [217] and to study the effects of applying an alternating electric field-based therapy to cancer cells [218]. To the best of our knowledge, integration of nanofibers at controlled spacing and orientations in a microfluidic device has yet to be demonstrated. If successful, such a platform can elucidate force coupling-based invasion of single and collection of cells in simultaneous biophysical and biochemical gradients. Furthermore, these models can be expanded to include stromal interactions by co-culturing fibroblasts and macrophages with and within the vicinity of cancerous cells to interrogate invasion dynamics.

Altogether, cancer affects all of us, and defeating it requires a concerted effort from all disciplines. Recent advancements in data mining, supercomputing, nanotechnologies, synthetic biology, molecular profiling, and social awareness provide us with a great hope in defeating cancer. Cancer will inevitably strike again; thus, we emphasize the need for collaborative research to understand the governing principles that make a cell go rogue and engineer ways to isolate and stop them in their tracks.

References

1. Mehlen P, Puisieux A (2006) Metastasis: a question of life or death. Nat Rev Cancer 6:449–458
2. Chen C-L et al (2013) Single-cell analysis of circulating tumor cells identifies cumulative expression patterns of EMT-related genes in metastatic prostate cancer. Prostate 73:813–826
3. Thiery JP, Acloque H, Huang RYJ, Nieto MA (2009) Epithelial-mesenchymal transitions in development and disease. Cell 139:871–890
4. Theveneau E et al (2013) Chase-and-run between adjacent cell populations promotes directional collective migration. Nat Cell Biol 15:763–772
5. Condeelis J, Segall JE (2003) Intravital imaging of cell movement in tumours. Nat Rev Cancer 3:921–930
6. Alexander DC et al (2010) Orientationally invariant indices of axon diameter and density from diffusion MRI. Neuroimage 52:1374–1389
7. Gritsenko PG, Ilina O, Friedl P (2012) Interstitial guidance of cancer invasion. J Pathol 226:185–199
8. Goetz JG et al (2011) Biomechanical remodeling of the microenvironment by stromal caveolin-1 favors tumor invasion and metastasis. Cell 146:148–163
9. Provenzano PP, Keely PJ (2011) Mechanical signaling through the cytoskeleton regulates cell proliferation by coordinated focal adhesion and Rho GTPase signaling. J Cell Sci 124:1195–1205
10. Provenzano PP, Keely PJ (2009) The role of focal adhesion kinase in tumor initiation and progression. Cell Adh Migr 3
11. Conklin MW et al (2011) Aligned collagen is a prognostic signature for survival in human breast carcinoma. Am J Pathol 178:1221–1232
12. Ilina O, Friedl P (2009) Mechanisms of collective cell migration at a glance. J Cell Sci 122:3203–3208
13. Aman A, Piotrowski T (2010) Cell migration during morphogenesis. Dev Biol 341:20–33
14. Wolf K et al (2007) Multi-step pericellular proteolysis controls the transition from individual to collective cancer cell invasion. Nat Cell Biol 9:893–904
15. Lauffenburger DA, Horwitz AF (1996) Cell migration: a physically integrated molecular process. Cell 84:359–369
16. Friedl P, Wolf K (2010) Plasticity of cell migration: a multiscale tuning model. J Cell Biol
17. Reig G, Pulgar E, Concha ML (2014) Cell migration: from tissue culture to embryos. Development 141:1999–2013
18. MacHacek M et al (2009) Coordination of Rho GTPase activities during cell protrusion. Nature 461:99–103
19. Petrie RJ, Gavara N, Chadwick RS, Yamada KM (2012) Nonpolarized signaling reveals two distinct modes of 3D cell migration. J Cell Biol 197
20. Hung W-C et al (2013) Distinct signaling mechanisms regulate migration in unconfined versus confined spaces. J Cell Biol 202:807–824
21. Petrie RJ, Doyle AD, Yamada KM (2009) Random versus directionally persistent cell migration. Nat Rev Mol Cell Biol 10:538–549
22. Even-Ram S, Yamada KM (2005) Cell migration in 3D matrix. Curr Opin Cell Biol 17:524–532
23. Doyle AD, Wang FW, Matsumoto K, Yamada KM (2009) One-dimensional topography underlies three-dimensional fibrillar cell migration. J Cell Biol 184
24. Friedl P, Sahai E, Weiss S, Yamada KM (2012) New dimensions in cell migration. Nat Rev Mol Cell Biol 13:743–747
25. Ridley AJ et al (2003) Cell migration: integrating signals from front to back. Science 302:1704–1709
26. Wade RJ, Burdick JA (2012) Engineering ECM signals into biomaterials. Mater Today 15:454–459
27. Zhang Y, Ouyang H, Lim CT, Ramakrishna S, Huang Z-M (2005) Electrospinning of gelatin fibers and gelatin/PCL composite fibrous scaffolds. J Biomed Mater Res 72B:156–165
28. Bosman FT, Stamenkovic I (2003) Functional structure and composition of the extracellular matrix. J Pathol 200:423–428
29. Schuppan D (1990) Structure of the extracellular matrix in normal and fibrotic liver: collagens and glycoproteins. Semin Liver Dis 10:1–10
30. Theocharis AD, Skandalis SS, Gialeli C, Karamanos NK (2016) Extracellular matrix structure. Adv Drug Deliv Rev 97:4–27
31. Frantz C, Stewart KM, Weaver VM (2010) The extracellular matrix at a glance. J Cell Sci 123
32. Cox BA, Starcher BC, Urry DW (1974) Communication coacervation of tropoelastin results in fiber formation. J Biol Chem 249:997–998
33. Zoumi A, Yeh A, Tromberg BJ (2002) Imaging cells and extracellular matrix in vivo by using second-harmonic generation and two-photon excited fluorescence. Proc Natl Acad Sci U S A 99:11014–11019
34. Patsialou A et al (2013) Intravital multiphoton imaging reveals multicellular streaming as a crucial component of in vivo cell migration in human breast tumors. IntraVital 2:e25294
35. Huang L, Apkarian RP, Chaikof EL (2006) High-resolution analysis of engineered type I collagen nanofibers by electron microscopy. Scanning 23:372–375
36. Oconnell M et al (2008) The three-dimensional micro- and nanostructure of the aortic medial lamellar unit measured using 3D confocal and electron microscopy imaging. Matrix Biol 27:171–181
37. Fernández M et al (2002) Small-angle x-ray scattering studies of human breast tissue samples. Phys Med Biol 47:577–592
38. Sharma P, Sheets K, Elankumaran S, Nain AS (2013) The mechanistic influence of aligned

nanofibers on cell shape, migration and blebbing dynamics of glioma cells. Integr Biol 5:1036–1044
39. Ushiki T (2002) Collagen fibers, reticular fibers and elastic fibers. A comprehensive understanding from a morphological viewpoint. Arch Histol Cytol 65:109–126
40. Montgomery H et al (2012) Proteomic profiling of breast tissue collagens and site-specific characterization of hydroxyproline residues of collagen alpha-1-(I). J Proteome Res 11:5890–5902
41. Friedl P, Wolf K (2009) Proteolytic interstitial cell migration: a five-step process. Cancer Metastasis Rev 28:129–135
42. Muiznieks LD, Keeley FW (2012) Molecular assembly and mechanical properties of the extracellular matrix : a fibrous protein perspective. Biochim Biophys Acta 1832:866–875
43. Gosline J et al (2002) Elastic proteins: biological roles and mechanical properties. Philos Trans R Soc Lond B Biol Sci 357:121–132
44. Dutov P, Antipova O, Varma S, Orgel JPRO, Schieber JD (2016) Measurement of elastic modulus of collagen type i single fiber. PLoS One 11:1–13
45. Kannus P, Kannus P (2000) Structure of the tendon connective tissue. Scand J Med Sci Sport 10:312–320
46. Raoufi M et al (2015) Nanopore diameters tune strain in extruded fibronectin fibers. Nano Lett 15:6357–6364
47. Chen LB, Murray A, Segal RA, Bushnell A, Walsh ML (1978) Studies on intercellular LETS glycoprotein matrices. Cell 14:377–391
48. Bradshaw MJ, Cheung MC, Ehrlich DJ, Smith ML (2012) Using molecular mechanics to predict bulk material properties of fibronectin fibers. PLoS Comput Biol 8
49. Klotzsch E et al (2009) Fibronectin forms the most extensible biological fibers displaying switchable force-exposed cryptic binding sites. Proc Natl Acad Sci U S A 106:18267–18272
50. LeBleu VS, Macdonald B, Kalluri R (2007) Structure and function of basement membranes. Exp Biol Med (Maywood) 232:1121–1129
51. Harley B a C et al (2008) Microarchitecture of three-dimensional scaffolds influences cell migration behavior via junction interactions. Biophys J 95:4013–4024
52. Carey SP, Kraning-Rush CM, Williams RM, Reinhart-King C a (2012) Biophysical control of invasive tumor cell behavior by extracellular matrix microarchitecture. Biomaterials 33:4157–4165
53. Paul CD, Mistriotis P, Konstantopoulos K (2016) Cancer cell motility: lessons from migration in confined spaces. Nat Rev Cancer 17:131–140
54. Huang Z-M, Zhang Y-Z, Kotaki M, Ramakrishna S (2003) A review on polymer nanofibers by electrospinning and their applications in nanocomposites. Compos Sci Technol 63:2223–2253
55. Li D, Xia Y (2004) Electrospinning of nanofibers: reinventing the wheel? Adv Mater 16:1151–1170
56. Matthews JA, Wnek GE, Simpson DG, Bowlin GL (2002) Electrospinning of collagen nanofibers. Biomacromolecules 3:232–238
57. Sun D, Chang C, Li S, Lin L (2006) Near-field electrospinning. Nano Lett 6:839–842
58. Chang C, Limkrailassiri K, Lin L (2008) Continuous near-field electrospinning for large area deposition of orderly nanofiber patterns. Appl Phys Lett 93:123111
59. Brown TD, Dalton PD, Hutmacher DW (2011) Direct writing by way of melt electrospinning. Adv Mater 23:5651–5657
60. Brown TD et al (2012) Design and fabrication of tubular scaffolds via direct writing in a melt electrospinning mode. Biointerphases 7:1–16
61. Badrossamay MR, McIlwee HA, Goss J a, Parker KK (2010) Nanofiber assembly by rotary jet-spinning. Nano Lett 10:2257–2261
62. Badrossamay MR et al (2014) Engineering hybrid polymer-protein super-aligned nanofibers via rotary jet spinning. Biomaterials 35:3188–3197
63. Deravi LF, Sinatra NR, Chantre CO, Nesmith AP, Yuan H, Deravi SK, Goss JA, MacQueen LA, Badrossamy MR, Gonzalez GM, Phillips MD, Parker KK (2017) Design and fabrication of fibrous nanomaterials using pull spinning. Macromol Mat Eng 302:1–14
64. Harfenist SA et al (2004) Direct drawing of suspended filamentary micro- and nanostructures from liquid polymers. Nano Lett 4:1931–1937
65. Nain AS, Sitti M, Jacobson A, Kowalewski T, Amon C (2009) Dry spinning based spinneret based tunable engineered parameters (STEP) technique for controlled and aligned deposition of polymeric nanofibers. Macromol Rapid Commun 30:1406–1412
66. Wang J, Nain AS (2014) Suspended micro/nanofiber hierarchical biological scaffolds fabricated using non-electrospinning STEP technique. Langmuir 30:13641–13649
67. Nain AS, Wang J (2013) Polymeric Nanofibers: isodiametric design space and methodology for depositing aligned nanofiber arrays in single and multiple layers. Polym J 451:695–700
68. Nain AS et al (2008) Control of cell behavior by aligned micro/nanofibrous biomaterial scaffolds fabricated by spinneret-based tunable engineered parameters (STEP) technique. Small 4:1153–1159
69. Pathak A, Kumar S (2011) Biophysical regulation of tumor cell invasion: moving beyond matrix stiffness. Integr Biol (Camb) 3:267–278
70. Baker BM, Chen CS (2012) Deconstructing the third dimension: how 3D culture microenvironments alter cellular cues. J Cell Sci 125:3015–3024
71. Friedl P, Alexander S (2011) Cancer invasion and the microenvironment: plasticity and reciprocity. Cell 147:992–1009

72. Rao SS et al (2013) Mimicking white matter tract topography using core-shell electrospun nanofibers to examine migration of malignant brain tumors. Biomaterials 34:5181–5190
73. Rao SS, Lannutti JJ, Viapiano MS, Sarkar A, Winter JO (2014) Toward 3D biomimetic models to understand the behavior of glioblastoma multiforme cells. Tissue Eng Part B Rev 20:314–327
74. Signaling S et al (2011) Glioma cell migration on three-dimensional nanofiber scaffolds is regulated by substrate topography and abolished by inhibition. Neoplasia 13:831–840
75. Rieger KA, Birch NP, Schiffman JD (2013) Designing electrospun nanofiber mats to promote wound healing – a review. J Mater Chem B 1:4531
76. Sheets K, Wunsch S, Ng C, Nain AS (2013) Shape-dependent cell migration and focal adhesion organization on suspended and aligned nanofiber scaffolds. Acta Biomater 9:7169–7177
77. McKee MG, Wilkes GL, Colby RJ, Long TE (2004) Correlations of solution rheology with electrospun fiber formation of linear and branched polyesters. Macromolecules 37:1760–1767
78. Shenoy SL, Bates WD, Frisch HL, Wnek GE (2005) Role of chain entanglements on fiber formation during electrospinning of polymer solutions: good solvent, non-specific polymer–polymer interaction limit. Polymer 46:3372–3384
79. Gupta P, Elkins C, Long TE, Wilkes GL (2005) Electrospinning of linear homopolymers of poly(methyl methacrylate): exploring relationships between fiber formation, viscosity, molecular weight and concentration in a good solvent. Polymer 46:4799–4810
80. Lee KH, Kim HY, Bang HJ, Jung YH, Lee SG (2003) The change of bead morphology formed on electrospun polystyrene fibers. Polymer 44:4029–4034
81. Wang C, Hsu CH, Lin JH (2006) Scaling laws in electrospinning of polystyrene solutions. Macromolecules 39:7662–7672
82. Carnell LS, Siochi EJ, Holloway NM, Stephens RM, Rhim C, Niklason LE, Clark RL (2008) Aligned mats from electrospun single fibers. Macromolecules 41:5345–5349
83. Agarwal S, Greiner A, Wendorff JH (2013) Functional materials by electrospinning of polymers. Prog Polym Sci 38:963–991
84. Doshi J, Reneker DH (1995) Electrospinning process and applications of electrospun fibers. J Electrostat 35:151–160
85. Orlova Y, Magome N, Liu L, Chen Y, Agladze K (2011) Electrospun nanofibers as a tool for architecture control in engineered cardiac tissue. Biomaterials 32:5615–5624
86. Ramakrishna S, Fujihara K, Teo W-E, Lim T-C, Ma Z (2005) An introduction to electrospinning and nanofibers. World Scientific Publishing Co. Pte. Ltd.
87. Zhang Y, Lim CT, Ramakrishna S, Huang Z-M (2005) Recent development of polymer nanofibers for biomedical and biotechnological applications. J Mater Sci Mater Med 16:933–946
88. Deitzel J, Kleinmeyer J, Harris D, Beck Tan N (2001) The effect of processing variables on the morphology of electrospun nanofibers and textiles. Polymer (Guildf) 42:261–272
89. Deitzel J (2001) Controlled deposition of electrospun poly(ethylene oxide) fibers. Polymer (Guildf) 42:8163–8170
90. Fridrikh SV, Yu JH, Brenner MP, Rutledge GC (2003) Controlling the fiber diameter during electrospinning. Phys Rev Lett 90(144502)
91. Theron SA, Yarin AL, Zussman E, Kroll E (2005) Multiple jets in electrospinning: experiment and modeling. Polymer (Guildf) 46:2889–2899
92. Theron SA, Zussman E, Yarin AL (2004) Experimental investigation of the governing parameters in the electrospinning of polymer solutions. Polymer (Guildf) 45:2017–2030
93. Ding B, Kimura E, Sato T, Fujita S, Shiratori S (2004) Fabrication of blend biodegradable nanofibrous nonwoven mats via multi-jet electrospinning. Polymer (Guildf) 45:1895–1902
94. Kidoaki S, Kwon IK, Matsuda T (2005) Mesoscopic spatial designs of nano- and microfiber meshes for tissue-engineering matrix and scaffold based on newly devised multilayering and mixing electrospinning techniques. Biomaterials 26:37–46
95. Kim G, Cho Y-S, Kim WD (2006) Stability analysis for multi-jets electrospinning process modified with a cylindrical electrode. Eur Polym J 42:2031–2038
96. Kumar A, Wei M, Barry C, Chen J, Mead J (2010) Controlling fiber repulsion in multijet electrospinning for higher throughput. Macromol Mater Eng 295:701–708
97. Srivastava Y, Marquez M, Thorsen T ((2007)) Multijet electrospinning of conducting nanofibers from microfluidic manifolds. J Appl Polym Sci 106(5):3171–3178. https://doi.org/10.1002/app.26810
98. Varesano A, Rombaldoni F, Mazzuchetti G, Tonin C, Comotto R (2010) Multi-jet nozzle electrospinning on textile substrates: observations on process and nanofibre mat deposition. Polym Int 59:1606–1615
99. Theron A, Zussman E, Yarin A (2001) Electrostatic field-assisted alignment of electrospun nanofibres. Nanotechnology 12:384–390
100. Sarkar S, Deevi S, Tepper G (2007) Biased AC Electrospinning of aligned polymer nanofibers. Macromol Rapid Commun 28:1034–1039
101. Hellmann C et al (2009) High precision deposition electrospinning of nanofibers and nanofiber nonwovens. Polymer (Guildf) 50:1197–1205
102. Li D, Wang Y, Xia Y (2003) Electrospinning of polymeric and ceramic nanofibers as uniaxially aligned arrays. Nano Lett 3:1167–1171

103. Li D, Xia Y (2003) Fabrication of titania nanofibers by electrospinning. Nano Lett 3:555–560
104. Larsen G, Velarde-Ortiz R, Minchow K, Barrero A, Loscertales IG (2003) A method for making inorganic and hybrid (organic/inorganic) fibers and vesicles with diameters in the submicrometer and micrometer range via sol−gel chemistry and electrically forced liquid jets. J Am Chem Soc 125:1154–1155
105. Viswanathamurthi P et al (2003) Preparation and morphology of niobium oxide fibres by electrospinning. Chem Phys Lett 374:79–84
106. Dai H, Gong J, Kim H, Lee D (2002) A novel method for preparing ultra-fine alumina-borate oxide fibres via an electrospinning technique. Nanotechnology 13:674–677
107. Katta P, Alessandro M, Ramsier RD, Chase GG (2004) Continuous electrospinning of aligned polymer nanofibers onto a wire drum collector. Nano Lett 4:2215–2218
108. Li D, Ouyang G, McCann JT, Xia Y (2005) Collecting electrospun nanofibers with patterned electrodes. Nano Lett 5:913–916
109. Zussman E, Theron A, Yarin AL (2003) Formation of nanofiber crossbars in electrospinning. Appl Phys Lett 82:973–975
110. Mellado P et al (2011) A simple model for nanofiber formation by rotary jet-spinning. Appl Phys Lett 99:1–3
111. Golecki HM et al (2014) Effect of solvent evaporation on fiber morphology in rotary jet spinning. Langmuir 30:13369–13374
112. van der Walt C, Hulsen M a, Bogaerds a CB, Anderson PD (2014) Transient modeling of fiber spinning with filament pull-out. J Nonnewton Fluid Mech 208–209:72–87
113. Deravi LF et al (2017) Design and fabrication of fibrous nanomaterials using pull spinning. Macromol Mater Eng 302:1–14
114. Nain, A. S. & Sitti, M. 3-D nano-fiber manufacturing by controlled pulling of liquid polymers using nano-probes. In 2003 Third IEEE conference on nanotechnology, 2003 IEEE-NANO 2003, vol 2, pp 60–63 (IEEE, 2003)
115. Nain AS, Amon C, Sitti M (2006) Proximal probes based nanorobotic drawing of polymer micro/nanofibers. IEEE Trans Nanotechnol 5:499–510
116. Nain AS, Wong JC, Amon C, Sitti M (2006) Drawing suspended polymer micro-/nanofibers using glass micropipettes. Appl Phys Lett 89:183105
117. Wang J, Hou J, Marquez E, Moore RB, Nain AS (2014) Aligned assembly of nano and microscale polystyrene tubes with controlled morphology. Polym (United Kingdom) 55
118. Christopherson GT, Song H, Mao H-Q (2009) The influence of fiber diameter of electrospun substrates on neural stem cell differentiation and proliferation. Biomaterials 30:556–564
119. Mo XM, Xu CY, Kotaki M, Ramakrishna S (2004) Electrospun P(LLA-CL) nanofiber: a biomimetic extracellular matrix for smooth muscle cell and endothelial cell proliferation. Biomaterials 25:1883–1890
120. Bashur CA, Dahlgren LA, Goldstein AS (2006) Effect of fiber diameter and orientation on fibroblast morphology and proliferation on electrospun poly(D,L-lactic-co-glycolic acid) meshes. Biomaterials 27:5681–5688
121. Badami A, Kreke M, Thompson MS, Riffle J, Goldstein A (2006) Effect of fiber diameter on spreading, proliferation, and differentiation of osteoblastic cells on electrospun poly(lactic acid) substrates. Biomaterials 27:596–606
122. Wang HB, Mullins ME, Cregg JM, McCarthy CW, Gilbert RJ (2010) Varying the diameter of aligned electrospun fibers alters neurite outgrowth and Schwann cell migration. Acta Biomater 6:2970–2978
123. Jin H-J, Chen J, Karageorgiou V, Altman GH, Kaplan DL (2004) Human bone marrow stromal cell responses on electrospun silk fibroin mats. Biomaterials 25:1039–1047
124. Prabhakaran MP, Venugopal JR, Ramakrishna S (2009) Mesenchymal stem cell differentiation to neuronal cells on electrospun nanofibrous substrates for nerve tissue engineering. Biomaterials 30:4996–5003
125. Yang F, Murugan R, Ramakrishna S (2005) Electrospinning of nano/micro scale poly(l-lactic acid) aligned fibers and their potential in neural tissue engineering. Biomaterials 26:2603–2610
126. Xue J et al (2017) Differentiation of bone marrow stem cells into Schwann cells for the promotion of neurite outgrowth on electrospun fibers. ACS Appl Mater Interfaces 9(14):12299–12310. https://doi.org/10.1021/acsami.7b00882
127. Nelson MT et al (2014) Preferential, enhanced breast cancer cell migration on biomimetic electrospun nanofiber 'cell highways'. BMC Cancer 14(825)
128. Saha S et al (2012) Electrospun fibrous scaffolds promote breast cancer cell alignment and epithelial-mesenchymal transition. Langmuir 28:2028–2034
129. Johnson J et al (2009) Quantitative analysis of complex glioma cell migration on electrospun polycaprolactone using time-lapse microscopy. Tissue Eng Part C Methods 15:531–540
130. Beliveau A, Thomas G, Gong J, Wen Q, Jain A (2016) Aligned nanotopography promotes a migratory state in glioblastoma multiforme tumor cells. Sci Rep 6:1–13
131. Alfano M et al (2016) Linearized texture of three-dimensional extracellular matrix is mandatory for bladder cancer cell invasion. Sci Rep 6(36128)
132. Koons B, Sharma P, Ye Z, Mukherjee A, Lee MH, Wirtz D, Behkam B, Nain AS (2017) Cancer protrusions on a tightrope—nanofiber curvature platform

reveals protrusion dynamics independent of cell migration. ACS Nano 11(12):12037–12048
133. Sheets K, Wang J, Zhao W, Kapania R, Nain AS (2016) Nanonet Force Microscopy for measuring cell forces. Biophys J 111:197–207
134. Meehan S, Nain AS (2014) Role of suspended fiber structural stiffness and curvature on single-cell migration, nucleus shape, and focal-adhesion-cluster length. Biophys J 107:2604–2611
135. Hall A et al (2017) Nanonet force microscopy for measuring forces in single smooth muscle cells of the human aorta. Mol Biol Cell 28:1894–1900
136. Starke J, Maaser K, Wehrle-Haller B, Friedl P (2013) Mechanotransduction of mesenchymal melanoma cell invasion into 3D collagen lattices: filopod-mediated extension–relaxation cycles and force anisotropy. Exp Cell Res 319:2424–2433
137. Bakhru S et al (2011) Direct and cell signaling-based, geometry-induced neuronal differentiation of neural stem cells. Integr Biol 3:1207–1214
138. Ker EDF et al (2011) Bioprinting of growth factors onto aligned sub-micron fibrous scaffolds for simultaneous control of cell differentiation and alignment. Biomaterials 32:8097–8107
139. Javier Bravo-Cordero J et al (2011) Directed cell invasion and migration during metastasis. This review comes from a themed issue on cell regulation edited introduction to cancer metastasis. Curr Opin Cell Biol 24:277–283
140. Lu P, Weaver VM, Werb Z (2012) The extracellular matrix: a dynamic niche in cancer progression. J Cell Biol 196:395–406
141. Sunyer R, Jin AJ, Nossal R, Sackett DL (2012) Fabrication of hydrogels with steep stiffness gradients for studying cell mechanical response. PLoS One 7:e46107
142. Rao SS et al (2012) Inherent interfacial mechanical gradients in 3D hydrogels influence tumor cell behaviors. PLoS One 7:e35852
143. Taddei ML, Giannoni E, Comito G, Chiarugi P (2013) Microenvironment and tumor cell plasticity: an easy way out. Cancer Lett 341:80–96
144. Brábek J, Mierke CT, Rösel D, Veselý P, Fabry B (2010) The role of the tissue microenvironment in the regulation of cancer cell motility and invasion. Cell Commun Signal 8:22
145. Hielscher AC, Qiu C, Gerecht S (2012) Breast cancer cell-derived matrix supports vascular morphogenesis. Am J Physiol Cell Physiol 302:C1243–C1256
146. Patsialou A et al (2012) Selective gene-expression profiling of migratory tumor cells in vivo predicts clinical outcome in breast cancer patients. Breast Cancer Res 14:R139
147. Palmer TD, Ashby WJ, Lewis JD, Zijlstra A (2011) Targeting tumor cell motility to prevent metastasis. Adv Drug Deliv Rev 63:568–581
148. Albuschies, J. & Vogel, V. The role of filopodia in the recognition of nanotopographies. https://doi.org/10.1038/srep01658
149. Adams JC (2001) Cell-matrix contact structures. Cell Mol Life Sci 58:371–392
150. Faix J, Breitsprecher D, Stradal TEB, Rottner K (2009) Filopodia: complex models for simple rods. Int J Biochem Cell Biol 41:1656–1664
151. Murphy DA, Courtneidge SA (2011) The 'ins' and 'outs' of podosomes and invadopodia: characteristics, formation and function. Nat Publ Gr 12
152. Clainche, C. L. E. & Carlier, M. Regulation of actin assembly associated with protrusion and adhesion in cell migration. 489–513 (2008). https://doi.org/10.1152/physrev.00021.2007.
153. Klemke RL (2012) Trespassing cancer cells: 'fingerprinting' invasive protrusions reveals metastatic culprits. Curr Opin Cell Biol 24:662–669
154. Condeelis JS et al (2001) Lamellipodia in invasion. Semin Cancer Biol 11:119–128
155. Friedl P, Wolf K (2003) Tumour-cell invasion and migration: diversity and escape mechanisms. Nat Rev Cancer 3:362–374
156. Wolf K, Friedl P (2011) Extracellular matrix determinants of proteolytic and non-proteolytic cell migration. Trends Cell Biol 21:736–744
157. Schoumacher M, Goldman RD, Louvard D, Vignjevic DM (2010) Actin, microtubules, and vimentin intermediate filaments cooperate for elongation of invadopodia. J Cell Biol 189
158. Woodward JKL et al (2002) An in vitro assay to assess uveal melanoma invasion across endothelial and basement membrane barriers. Invest Ophthalmol Vis Sci 43:1708–14 (
159. Oppegard SC, Blake AJ, Williams JC, Eddington DT (2010) Precise control over the oxygen conditions within the Boyden chamber using a microfabricated insert. Lab Chip 10:2366–2373
160. Souchet M et al (2002) Human p63RhoGEF, a novel RhoA-specific guanine nucleotide exchange factor, is localized in cardiac sarcomere. J Cell Sci 115:629–640
161. Burnette DT et al (2011) A role for actin arcs in the leading-edge advance of migrating cells. Nat Cell Biol 13:371–381
162. Gov NS, Gopinathan A (2006) Dynamics of membranes driven by actin polymerization. Biophys J 90:454–469
163. Ponti A, Machacek M, Gupton SL, Waterman-Storer CM, Danuser G ((2004)) Two distinct actin networks drive the protrusion of migrating cells. Science 305:1782–1786
164. Zicha D et al (2003) Rapid actin transport during cell protrusion. Science 300:142–145
165. Meyer AS et al (2012) 2D protrusion but not motility predicts growth factor-induced cancer cell migration in 3D collagen. J Cell Biol 197:721–729
166. Alexandrova AY et al (2008) Comparative dynamics of retrograde actin flow and focal adhesions: formation of nascent adhesions triggers transition from fast to slow flow. PLoS One 3:e3234

167. Vicente-Manzanares M, Ma X, Adelstein RS, Horwitz AR (2009) Non-muscle myosin II takes centre stage in cell adhesion and migration. Nat Rev Mol Cell Biol 10:778–790
168. Pollard TD, Borisy GG (2003) Cellular motility driven by assembly and disassembly of actin filaments. Cell 112:453–465
169. Zimmermann J, Falcke M, Frey E, Engel H, Eiswirth M (2014) Formation of transient lamellipodia. PLoS One 9:e87638
170. Yang C, Svitkina T (2011) Filopodia initiation. Cell Adh Migr 5:402–408
171. Mattila PK, Lappalainen P (2008) Filopodia: molecular architecture and cellular functions. Nat Rev Mol Cell Biol 9:446–454
172. Svitkina TM et al (2003) Mechanism of filopodia initiation by reorganization of a dendritic network. J Cell Biol 160
173. Alblazi K, Siar C (2015) Cellular protrusions—lamellipodia, filopodia, invadopodia and podosomes—and their roles in progression of orofacial tumours: current understanding. Asian Pac J Cancer Prev 16:2187–2191
174. Fraley SI et al (2010) A distinctive role for focal adhesion proteins in three-dimensional cell motility. Nat Cell Biol 12:598–604
175. Petrie RJ, Koo H, Yamada KM (2014) Generation of compartmentalized pressure by a nuclear piston governs cell motility in a 3D matrix. Science 345:1062–1065
176. Giri A et al (2013) The Arp2/3 complex mediates multigeneration dendritic protrusions for efficient 3-dimensional cancer cell migration. FASEB J 27:4089–4099
177. Yap B, Kamm RD (2005) Mechanical deformation of neutrophils into narrow channels induces pseudopod projection and changes in biomechanical properties. J Appl Physiol 98
178. Linder S, Aepfelbacher M (2003) Podosomes: adhesion hot-spots of invasive cells. Trends Cell Biol 13:376–385
179. Linder S (2007) The matrix corroded: podosomes and invadopodia in extracellular matrix degradation. Trends Cell Biol 17:107–117
180. Gimona M, Buccione R, Courtneidge SA, Linder S (2008) Assembly and biological role of podosomes and invadopodia. Curr Opin Cell Biol 20:235–241
181. Artym VV, Zhang Y, Seillier-Moiseiwitsch F, Yamada KM, Mueller SC (2006) Dynamic interactions of cortactin and membrane type 1 matrix metalloproteinase at invadopodia: defining the stages of invadopodia formation and function. Cancer Res 66
182. Weaver AM (2006) Invadopodia: specialized cell structures for cancer invasion. Clin Exp Metastasis 23:97–105
183. Buccione R, Orth JD, McNiven MA (2004) Foot and mouth: podosomes, invadopodia and circular dorsal ruffles. Natl Rev 5:647–657
184. Ohnishi T et al (1998) Role of fibronectin-stimulated tumor cell migration in glioma invasion in vivo: clinical significance of fibronectin and fibronectin receptor expressed in human glioma tissues. Clin Exp Metastasis 16:729–741
185. Rape A, Ananthanarayanan B, Kumar S (2014) Engineering strategies to mimic the glioblastoma microenvironment. Adv Drug Deliv Rev 79–80:172–183
186. Fernandez-Garcia B et al (2014) Expression and prognostic significance of fibronectin and matrix metalloproteases in breast cancer metastasis. Histopathology 64:512–522
187. Park J, Schwarzbauer JE (2014) Mammary epithelial cell interactions with fibronectin stimulate epithelial-mesenchymal transition. Oncogene 33:1649–1657
188. Roussos ET, Condeelis JS, Patsialou A (2011) Chemotaxis in cancer. Nat Rev Cancer 11:573–587
189. Sharma P et al (2017) Aligned fibers direct collective cell migration to engineer closing and nonclosing wound gaps. Mol Biol Cell 28:2579–2588
190. Estabridis HM, Jana A, Nain A, Odde DJ (2018) Cell migration in 1D and 2D nanofiber microenvironments. Ann Biomed Eng 46:392–403
191. Clark RAF et al (1982) Fibronectin and fibrin provide a provisional matrix for epidermal cell migration during wound reepithelialization. J Invest Dermatol 79:264–269
192. Cavani A et al (1993) Distinctive integrin expression in the newly forming epidermis during wound healing in humans. J Invest Dermatol 101:600–604
193. Krawczyk WS (1971) A pattern of epidermal cell migration during wound healing. J Cell Biol 49:247–263
194. Pollard TD, Blanchoin L, Mullins RD (2000) Molecular mechanisms controlling actin filament dynamics in nonmuscle cells. Annu Rev Biophys Biomol Struct 29:545–576
195. Yamazaki D, Kurisu S, Takenawa T (2005) Regulation of cancer cell motility through actin reorganization. Cancer Sci 96:379–386
196. Paňková K, Rösel D, Novotný M, Brábek J (2010) The molecular mechanisms of transition between mesenchymal and amoeboid invasiveness in tumor cells. Cell Mol Life Sci 67:63–71
197. Wang W et al (2002) Single cell behavior in metastatic primary mammary tumors correlated with gene expression patterns revealed by molecular profiling. Cancer Res 62:6278–6288
198. Wolf K et al (2003) Compensation mechanism in tumor cell migration. J Cell Biol 160
199. Friedl P, Borgmann S, Bröcker EB (2001) Amoeboid leukocyte crawling through extracellular matrix: lessons from the Dictyostelium paradigm of cell movement. J Leukoc Biol 70:491–509
200. Charras G, Paluch E (2008) Blebs lead the way: how to migrate without lamellipodia. Nat Rev Mol Cell Biol 9:730–736

201. Babiychuk EB, Monastyrskaya K, Potez S, Draeger A (2011) Blebbing confers resistance against cell lysis. Cell Death Differ 18:80–89
202. Fackler OT, Grosse R (2008) Cell motility through plasma membrane blebbing. J Cell Biol 181
203. Paluch EK, Raz E (2013) The role and regulation of blebs in cell migration. Curr Opin Cell Biol 25:582–590
204. Bergert M, Chandradoss SD, Desai RA, Paluch E (2012) Cell mechanics control rapid transitions between blebs and lamellipodia during migration. Proc Natl Acad Sci U S A 109:14434–14439
205. Paszek MJ, Weaver VM (2004) The tension mounts: mechanics meets morphogenesis and malignancy. J Mammary Gland Biol Neoplasia 9:325–342
206. Croft DR et al (2004) Conditional ROCK activation in vivo induces tumor cell dissemination and angiogenesis. Cancer Res 64:8994–9001
207. Joyce J a, Pollard JW (2009) Microenvironmental regulation of metastasis. Nat Rev Cancer 9:239–252
208. Kumar S, Weaver VM (2009) Mechanics, malignancy, and metastasis: the force journey of a tumor cell. Cancer Metastasis Rev 28:113–127
209. Jaffe AB, Hall A (2005) Rho GTPases: biochemistry and biology. Annu Rev Cell Dev Biol 21:247–269
210. Burridge K, Wennerberg K (2004) Rho and Rac take center stage. Cell 116:167–179
211. Petrie RJ, Yamada KM (2012) At the leading edge of three-dimensional cell migration. J Cell Sci 125:5917–5926
212. Friedl P (2004) Prespecification and plasticity: shifting mechanisms of cell migration. Curr Opin Cell Biol 16:14–23
213. Jeon NL et al (2000) Generation of solution and surface gradients using microfluidic systems. Langmuir 16:8311–8316
214. Whitesides GM (2006) The origins and the future of microfluidics. Nature 442:368–373
215. Traore MA, Behkam B (2013) A PEG-DA microfluidic device for chemotaxis studies. J Micromech Microeng 23:085014
216. Wheeler, A. R. et al. Microfluidic device for single-cell analysis. https://doi.org/10.1021/ac0340758
217. Boussommier-Calleja A, Kamm R (2017) Abstract B22: role of monocytes in 3D microfluidic models of cancer cell extravasation. Cancer Immunol Res 5
218. Pavesi A et al (2016) Engineering a 3D microfluidic culture platform for tumor-treating field application. Sci Rep 6
219. Sharma P et al (2014) Aligned and suspended fiber force probes for drug testing at single cell resolution. Biofabrication 6:045006